NASA TECHNICAL NOTE

NASA TN D-5528

NASA TN D-5528

A HARDWARE SIMULATION OF A LUNAR MIDCOURSE NAVIGATION SYSTEM USING STATISTICAL FILTER THEORY AND HAND-HELD SEXTANT OBSERVATIONS

by Jay V. Christensen and Leonard A. McGee

Ames Research Center
Moffett Field, Calif.

NATIONAL AERONAUTICS AND SPACE ADMINISTRATION • WASHINGTON, D. C. • NOVEMBER 1969

1. Report No.	2. Government Accession No.	3. Recipient's Catalog No.
NASA TN D-5528		

4. Title and Subtitle	5. Report Date
A HARDWARE SIMULATION OF A LUNAR MIDCOURSE NAVIGATION SYSTEM USING STATISTICAL FILTER THEORY AND HAND-HELD SEXTANT OBSERVATIONS	November 1969
	6. Performing Organization Code
7. Author(s)	8. Performing Organization Report No.
Jay V. Christensen and Leonard A. McGee	A-2841
9. Performing Organization Name and Address	10. Work Unit No.
NASA Ames Research Center Moffett Field, Calif., 94035	125-17-04-01-00-21
	11. Contract or Grant No.
	13. Type of Report and Period Covered
12. Sponsoring Agency Name and Address	TECHNICAL NOTE
National Aeronautics and Space Administration Washington, D. C., 20546	14. Sponsoring Agency Code

15. Supplementary Notes

16. Abstract

A simulation investigation is reported that considers the application of Kalman statistical filter theory and hand-held-sextant observations to lunar midcourse guidance and navigation. The specific system under investigation consisted of on-board guidance and navigation computations, a computer control and display system, and a hand-held sextant. An on-board digital computer was simulated using a ground-based digital computer, and the guidance and navigation computations were based on statistical filter theory and linear prediction. Symbolic abbreviation techniques were implemented in the control of the simulated on-board computer and to identify computer data. Observations of a simulated celestial scene were taken with a hand-held sextant which had been flown on the Gemini XII mission. The observer was a qualified Air Force navigator, and observations were taken under static conditions and under moving-planet and moving-cab conditions.

17. Key Words (Suggested by Authors)	18. Distribution Statement
Kalman statistical filter theory Midcourse navigation Computer control and display Hand-held sextant	Unclassified - Unlimited

19. Security Classif. (of this report)	20. Security Classif. (of this page)	21. No. of Pages	22. Price*
Unclassified	Unclassified	54	$3.00

*For sale by the Clearinghouse for Federal Scientific and Technical Information
Springfield, Virginia 22151

TABLE OF CONTENTS

A HARDWARE SIMULATION OF A LUNAR MIDCOURSE NAVIGATION SYSTEM USING STATISTICAL FILTER THEORY AND HAND-HELD SEXTANT OBSERVATIONS

By Jay V. Christensen and Leonard A. McGee

Ames Research Center

SUMMARY

A simulation investigation is reported that considers the application of Kalman statistical filter theory and hand-held-sextant observations to lunar midcourse guidance and navigation. The specific system under investigation consisted of on-board guidance and navigation computations, a computer control and display system, and a hand-held sextant. An on-board digital computer was simulated using a ground-based digital computer, and the guidance and navigation computations were based on statistical filter theory and linear prediction. Symbolic abbreviation techniques were implemented in the control of the simulated on-board computer and to identify computer data. Observations of a simulated celestial scene were taken with a hand-held sextant which had been flown on the Gemini XII mission. The observer was a qualified Air Force navigator, and observations were taken under static conditions and under moving-planet and moving-cab conditions.

Three sets of eight trajectory runs each were considered for the return, moon-to-earth, portion of a lunar mission in which inbound observations were processed and inbound velocity corrections were simulated. The resulting actual trajectories were compared with the on-board estimated trajectories, with the desired reference trajectory, and with theoretical reference data to obtain systems guidance and navigation performance data. The actual trajectories were also compared to acceptable reentry corridor requirements.

The results further confirm theoretical studies based on assumed-error models and indicate that an on-board system that utilizes hand-held-sextant observation data, processed by statistical filter techniques, and linear prediction, has the potential of providing acceptable guidance and navigation performance. No serious anomalies or discontinuities were detected in the use of statistical filter processing. Operational results obtained by a symbolic-alphabetic abbreviation technique were satisfactory.

INTRODUCTION

A number of theoretical studies have shown the potential advantages of applying statistical filter theory to lunar midcourse guidance and navigation (refs. 1, 2, and 3). These studies were based on processing observational

data that have an assumed theoretical error distribution. Also, a number of studies (refs. 4, 5, and 6) have illustrated the potential of using a hand-held sextant for space navigation and guidance.

To investigate the application of both these concepts, and to further investigate actual hardware, the present study considered system guidance and navigation performance of a specific hardware-computational system. The specific system investigated consisted of a simulated on-board digital computer, a digital computer control and display panel, and a flight-qualified hand-held sextant flown on the Gemini XII mission (refs. 7 and 8). On-board digital computations and data processing techniques were used. This investigation is essentially an extension of the research reported in reference 9, which investigated a similar system but used data from a theodolite operated manually from a fixed base.

Performance was evaluated for two environmental conditions: (1) ideal static conditions, where there is no motion of the cab or of the planet simulator; and (2) dynamic conditions, where the observations are taken when the cab and planet simulator are moving. Errors for such a system could also come from a number of other sources, such as sighting through a window, earth-landmark tracking uncertainties, velocity correction maneuver and measurement errors, shadow variations on the moon. However, such error sources were not considered in this study.

This study was conducted in three phases. Phase I considered performance starting with the last 12 observations, through the last velocity correction to perigee. The observation data utilized in this phase were taken by the observer in a simulated mission sequence. There were no dynamic motions involving the celestial scene or the simulated cab. Phase II included the the complete return trajectory and utilized observation data obtained from the Phase I investigations. Phase III considered the complete return trajectory but utilized observation data taken when the simulated planet was moving relative to the star scene and the simulated cab was rotating about all three axes. For Phase III, the observation data were not taken in a simulated mission sequence as in Phase I. The observation data set used in Phase III were obtained over a two-week period under dynamic planet and cab conditions typical of worst-case conditions expected during the midcourse phase. This technique saved considerable time and provided a practical way of investigating performance under moving line-of-sight and moving-cab conditions.

Each study phase consisted of eight data runs in which sextant observations were processed, velocity corrections were simulated, and the resulting trajectories were computed to vacuum perigee to determine system performance. Guidance and navigation performance analysis considered accuracy of the trajectory state estimation, the resulting velocity correction, the deviation of the actual trajectory from the reference trajectory, and the ability of the system to meet reentry trajectory state requirements at vacuum perigee. The guidance and navigation of the system was compared with theoretical performance of a system which uses identical computations and assumes sextant errors having standard deviations that bracket the performance of the actual sextant.

SYMBOLS

$A(t_e,t_1)$	prediction matrix (6 × 6) relating state at the end point t_e to that at t_1
A_1,A_2,A_3,A_4	submatrices (3 × 3) of A
F	matrix (6 × 6) of partial derivatives of the equation of motion with respect to the state variables
G	guidance matrix (6 × 6)
H	matrix (1 × 3) relating observed sextant angle and vehicle state
I	identity matrix with appropriate dimensions
K	Kalman weighting matrix (6 × 1)
P	covariance matrix (6 × 6) of estimation error
P'	new value of P after a sextant observation
P_1,P_2,P_3,P_4	submatrices (3 × 3) of P
Q	covariance matrix (1 × 1) of the observational errors
r	actual position deviation from reference (3 × 1 matrix)
$\tilde{r}$	error in estimate of r (3 × 1 matrix)
$\tilde{r}_{rms}$	rms value of the error in the estimate of r (3 × 1 matrix)
$\hat{r}$	estimate of r (3 × 1 matrix)
$\hat{r}_{rms}$	rms value of the estimate of r
R	covariance matrix (6 × 6) of the deviations between the actual and reference states
R'	new value of R (6 × 6) after a velocity correction
Δ	increment
η	Gaussian noise with zero mean
$\Phi(t_k,t_{k-1})$	transition matrix (6 × 6) relating state at t_k to state at t_{k-1}

Notation Conventions

$( )^T$	transpose of matrix ( )
$( )^{-1}$	inverse of matrix ( )
E[ ]	expected value of [ ]
trace [ ]	sum of the principal diagonal elements of [ ]
Δv_{rms}	rms value of the indicated velocity correction
ΔV	covariance matrix (3 × 3) of the indicated velocity correction
ΔV_G	velocity-vector increment (3 × 1 matrix) to be gained
$\lvert\Delta V_G\rvert$	magnitude of ΔV_G
x	six-vector (6 × 1) deviation of the actual position and velocity from a reference trajectory ($\hat{x} + \tilde{x}$)
$\hat{x}$	estimate (6 × 1) of x
$\tilde{x}$	error (6 × 1) in the estimate of x
X,Y,Z	Cartesian coordinates of vehicle's position
X_m, Y_m, Z_m	Cartesian coordinates of moon's position
X_S, Y_S, Z_S	Cartesian coordinates of sun's position
y	actual sextant space angle
$\hat{y}$	estimate of y

Subscripts and Matrix Arguments

e	end point
k	at the kth observation
t	general time arguments
t_e	end-point time
t_k	time of the kth observations
rms	root-mean-square value

SIMULATION DESCRIPTION

Specific hardware and an on-board computer simulation were used to investigate on-board techniques for navigation of manned spacecraft. The system evaluated in this investigation is illustrated in figure 1.

Hand-Held Sextant

The sighting instrument (fig. 2) was a hand-held sextant which had been flown on the Gemini XII mission. The general characteristics of the sextant follow:

Size: 7-1/4 × 6-1/16 in.
Weight: 6-1/2 oz
Magnification: 8×
Measurement range: 76°
Field of view: 7°

Reference 7 describes the sextant design and space-flight rating.

Computer Control and Display

The digital computer control and display panel concept was based on symbolic abbreviations. The display panel consisted of the following subassemblies as numbered in figure 3: (1) electroluminescent computer control mode lamps, (2) incandescent status and warning lights, (3) time interrogate pushbutton, (4) real-time clock display and control, (5) electroluminescent symbolic and numeric display panels, (6) single function, priority interrupt pushbutton panel, (7) thumbwheel input panel, and (8) keyboard input panel.

Details regarding the computer control and display panel concept, operation, data format requirements, symbolic code structure, computer memory requirements, and functional descriptions of the required programs are discussed in reference 9.

On-Board Digital Guidance and Navigation Computations

The on-board digital computer was simulated with a general-purpose, ground-based computer. The mathematical formulas and techniques for on-board guidance and navigation computations were essentially those used by Smith, McLean, Schmidt, and McGee (refs. 1, 2, and 3), and are discussed further in the section on digital computations. The integration technique, reported in reference 10, was a Stormer-Cowell integration with a starter that builds up the table of differences backwards in time from the point of integration. This particular technique was chosen to reduce integration error as much as possible. Knowledge of the position of the sun and moon was required, and a Tchebycheff polynomial in time was fitted to each Cartesian coordinate of the

sun-moon data over a 17-day time period. This time span was chosen to allow for the 7-day round-trip, launch delays, and stay-time on the moon. The polynomial coefficients were computed from Naval Observatory data.

For the on-board computer simulation, two sets of nonlinear equations of motion were computed and integrated: the reference trajectory set, which defined a nominal trajectory around which the equations of motion were linearized for prediction and guidance; and the estimated trajectory set, which was computed to obtain the best estimate of the position and velocity of the vehicle. The equations of motion included the effect of the sun, the moon, and the second harmonic of the earth's gravitational potential; these are summarized in appendix A. The coordinate system used was a nonrotating, right-hand orthogonal Cartesian frame with its origin at the center of the earth, as illustrated in appendix A.

SIMULATION CONFIGURATION AND TECHNIQUES

The simulation configuration is illustrated in figure 4. The computer control and display panel was mounted in a moving-base cab simulator, and observations of the simulated scene were tkaen by the observer under dynamic and static conditions.

Digital Computer Simulation

An SDS 920 computer was used to simulate the on-board computer and to perform the necessary calculations, calibrations, and data processing associated with the celestial scene and the computation of the research data. The computer system configuration is shown in figure 5. The simulation was a complete digital simulation. The digital central processor was a 24-bit, general-purpose machine with 12,288 words of random accessible storage. FORTRAN and symbolic programming techniques were used. The advantages of FORTRAN in meeting the complexity and scaling requirements of the guidance and navigation equations outweighed the problems of interfacing the FORTRAN with the machine language (symbolic) portions of the program. The real-time hardware systems, such as the computer control and display programs, real-time mission clock control and display, and celestial scene encoder interrogation, could only be controlled by symbolic machine language programs. They were written in symbolic language and called through interrupts or as FORTRAN subroutines. Storage of 24,000 words was required for the simulation; of this amount, 12,000 were required for the on-board system simulation. Since the total program exceeded core storage, it was necessary to fractionalize the program into links on the magnetic tape and call in portions as appropriate. Double-precision, floating-point programs having 11 significant decimal digits were used for all guidance and navigation computations. More details regarding the digital computer simulation techniques used are discussed in references 9 and 11.

Digital Computations

The digital computations used in this study were a modified version of those used for the midcourse navigation studies reported in reference 1. The reference mission was the return leg of a circumlunar trajectory. Imperfect injection conditions for the space vehicle at the perilune point were assumed, and the function of the navigation and guidance system was to cause the space vehicle to arrive at the reference end point (vacuum perigee) with a minimum of time and position error. The navigation system processed sextant observations of the angle between a known landmark and a known star at preselected times. From the resulting data, the system generated an estimate of the vehicle state (position and velocity) by means of a Kalman statistical filter. On the basis of this estimate, the guidance system executed exactly the estimated corrections to the vehicle velocity that were required in order for the vehicle to arrive at the reference end point (vacuum perigee).

Twenty-seven, second-order ordinary differential equations, comprising three trajectories and six sets of three perturbation equations, were integrated simultaneously. A numerical integration subroutine described in reference 10 was used in these computations.

For this simulation study, three trajectories were computed: (1) a previously determined *reference* trajectory, (2) an *estimated* trajectory giving the current estimate of the vehicle state, and (3) an *actual* trajectory giving the true state of the space vehicle. The reference and estimated trajectories were processed in the on-board computer simulation. The actual trajectory would not be available on board an actual spacecraft, so it was considered to have been computed external to the spacecraft. Comparison of statistical deviations between the states of these three trajectories permitted evaluations of the performance of the system with various sextant errors.

Figure 6 is a block diagram illustrating the computational flow: the bracketed numbers in the following discussion identify the steps in the digital computation process, and correspond with numbered boxes in the figure.

In this simulation investigation, when a sextant observation made at time t_k is to be processed, numerical integration of the equations of motion is initiated simultaneously [1], for the reference, actual, and estimated trajectories. The equations of motion and the coordinate system used are described in appendix A. Initial conditions for the actual and reference trajectories are merely the states that existed at the time of the last observation, whereas the estimated trajectory uses the new estimated state derived from processing the last sextant observation. Simultaneously with the integration of the equation of motion by the numerical technique of reference 10, the sixfold perturbation equations [2] are also integrated numerically from the time of the last observation t_{k-1}. This process continues until the computer time equals the time of the observation t_k. The integration is then stopped, and the transition matrix $\Phi(t_k,t_{k-1})$ is calculated [3] as described in appendix B.

A discussion of the mathematics used in the computations described in the remainder of this section is contained in appendix C.

The covariance matrix of the estimation error $P(t_k)$ and the covariance matrix of the deviations between the actual and the reference states $R(t_k)$ are updated [4] through linear prediction.

Next, the matrix H, relating the observed sextant angle to the vehicle state, is computed [5] so that the Kalman weighting matrix $K(t_k)$ may be obtained. The Kalman weighting matrix is computed [6] for this application in the form given in reference 1. With $K(t_k)$ known, the value of the covariance matrix of estimation error after a sextant observation $P'(t_k)$ is then computed [7]. The delay unit [8] represented the storage of $P(t_k)$ until the time of the next observation when it becomes $P(t_{k-1})$.

The next process is to compute the new estimated state through a series of steps. In this system, a sextant observation consists of measuring the angle between a chosen star and a chosen landmark. First, the estimated sextant angle is computed [9] from geometrical equations using the estimated position; then the actual sextant angle is computed [10] using the actual position. The estimated sextant angle is next subtracted from the actual sextant angle, and observation errors are added, which are based on the covariance matrix of the observational errors, Q, or on errors obtained by taking observations of a simulated celestial scene with an actual sextant. Finally, the result [11] multiplied by $K(t_k)$ [12] is added to the estimated state [13] to produce a new estimated state.

Next, the indicated velocity correction is computed by means of a prediction matrix $A(t_e,t_k)$, which predicts the end-point state from the present state [14]. Submatrices from $A(t_e,t_k)$ are used to compute a matrix G which is needed in computing the indicated velocity correction. The indicated velocity correction, ΔV_G, is computed by multiplying the difference between the reference state and the estimated state, $\hat{x}$ [15] by G [16]. The statistics of the indicated velocity correction are determined from a covariance matrix ΔV [17].

This concludes the computation cycle at each observation, and the computer is now ready to process the next observation unless a velocity correction is to be executed. In this case, the correction is made after a time delay simulating the time required to orient the vehicle along the desired thrust vector. Trajectory determination processes [1], [2], and [3] are continued until the computer time equals the time at which the velocity correction is to be made. Processes [4], [14], [15], and [16] are repeated, and computational control is passed to a separate program section for the performance of the velocity correction maneuver.

The flow lines that represent the velocity correction process are shown as dashed lines in figure 6 to emphasize the occasional nature of the velocity corrections. Also, these corrections are assumed to occur instantaneously so that no position or time change need be accounted for during the maneuver. The velocity correction results in a change in the subsequent actual

and the estimated states. To complete the velocity correction cycle, the R matrix, which is the covariance matrix of the errors between the actual and the estimated states, must be corrected to reflect the effects of the velocity correction maneuver [18]. The computation then proceeds to process the next observation.

Celestial Scene Simulation

Figure 7 is a photograph of a star simulator, which is a collimated point light source fixed with respect to the moon simulator base and the spacecraft cab simulator base. The moon simulator (fig. 8) projected a collimated photograph of the moon which subtended an angle of $1/2^{\circ}$ from limb to limb. The collimated image of the moon was either repositioned between observations or driven at a constant angular rate with respect to the fixed-star source. The moon simulator interfaced with the computer through a natural binary digital encoder that provided an angle readout resolution of 1.25 seconds of arc. Figure 9 is a view of the simulated celestial scene from the observer's station in the cab. In this study, angular travel was restricted under dynamic conditions to less than 7 minutes of arc to enhance accurate angle generation.

A set of 96 observations was taken of the moon and star simulator using the hand-held sextant under ideal static conditions (Phase I data). The resulting sextant error set had a mean of 2.5 seconds of arc and a standard deviation about the mean of 5.9 seconds of arc. A comparison of these results with those of reference 6 shows good correlation (5.9 sec error as compared with 4 and 5 sec). One can conclude then that very little random error was generated by the simulation of the celestial scene. The 2.5 seconds mean error may be assumed simulation calibration error or instrument calibration error. In both cases (random and mean error) it was felt that this magnitude of the simulation error was not large enough to compromise the results of the study.

Spacecraft Cab Simulation

The spacecraft cab simulator is shown in figure 10. The computer control and display panel was installed in the cab so the observer could control the simulated on-board computer (fig. 11). The hand-held sextant was suspended by a cable from the top of the observation window to reduce the fatigue effects of holding the instrument in a gravity field. Particular care was taken in this installation to reduce the possibility of adversely stressing the instrument. When observations were taken, the background lighting of the scene which was required to take the photographs of figures 7-11, was eliminated. The cab was mounted on an air-bearing to reduce friction and rotated about all three axes to simulate a limit-cycle condition for the dynamic phase of the simulation. An analog computer was used to generate appropriate signals for the servo-drive system that rotated the cab.

INVESTIGATION PROCEDURES

A representative moon-to-earth return mission and trajectory was chosen. The selected observation schedule, initial conditions, and system errors were typical of a moon-to-earth return guidance and navigation problem; however, no attempt was made to study or optimize these factors. The reference trajectory was the return portion of a free return circumlunar trajectory of a spacecraft launched from Cape Kennedy. Closest approach to the moon (perilune) was 185.3 km (100.0 nautical miles) from the surface. Vacuum perigee was 60.0 km above sea level at latitude 24.2° N, and longitude 80.98° W, which is approximately over Havana, Cuba.

All mission times were from translunar injection. The spacecraft injection at perilune takes place at 70.68 hours. Initial errors were identified by adding initial condition errors to the reference trajectory at the perilune mission time. A random number generator computed these initial condition errors on the basis of a normal error distribution with a standard deviation of 1 km and 0.001 km/sec in each Cartesian coordinate. The specific errors that resulted are given in table I.

Observation Procedures

Two types of observation sets were taken. One set was taken under static conditions where, prior to each observation, the moon simulator was positioned to a new angle unknown to the observer; motion of the celestial scene or the cab was not introduced. The other observation set was taken under dynamic conditions where cab motion and planet motion were introduced during the observation. During these dynamic observation data runs, the line-of-sight to the moon simulator was moving with respect to the fixed star simulator at 5 seconds of arc per second, which is considered a maximum rate for the midcourse phase.

All observations were taken with respect to the center of the moon crater Tycho (fig. 12). All observations and velocity corrections were based on fixed times as summarized in table II and illustrated in figure 13. An observation was taken by superimposing the star source and the center of the moon crater as seen through the sextant. In all cases, observations were taken with respect to the moon simulator even when the schedule called for an observation of the earth. When the observer was satisfied with the observation (i.e., when the targets were superimposed in the sextant sighting task), he actuated a mission time-interrogate pushbutton mounted on the sextant after which the sextant angle was not modified. The activation of the mission time-interrogate pushbutton initiated a computer program that stored the mission time of the observation to 0.01 second, interrogated the moon simulator digital encoder to determine the moon simulator angular position, and then computed the simulated celestial scene angle that existed at the time of the observation. The observer read the observed angle from the index readings on the sextant and entered it into the computer through the computer-control and display panel. This sextant observation angle was then compared with the moon

simulator angular position and the difference was taken as the error in the observation. When an earth observation was scheduled, the on-board computations processed the observations of the moon simulator as if the observations had been taken of the earth.

All three trajectories (estimated, reference, and actual) were then updated to the time of the observation, and the "actual" angle that should have been observed at that point from the actual trajectory was computed for the particular star and planet. The observation error was then algebraically added to the "actual" angle, and the resulting "observed" angle was then processed using the statistical filter theory. This simulation technique is discussed further in reference 9.

Velocity Correction Procedures

The velocity correction maneuver was simulated. The velocity correction magnitude and direction, as estimated by the on-board guidance and navigation computations, were used in the simulation. Errors in cutoff, alinement, and measurement were not introduced.

Study Phases

The three study phases are summarized as follows:

	Phase I	Phase II	Phase III
Mission segment	122.0 hr to perigee	70.68 hr to perigee	70.68 hr to perigee
Number of observations	12	39	39
Velocity corrections	Last inbound	All 3 inbound	All 3 inbound
Conditions under which the observations were taken	Static	Static (processed Phase I data)	Planet and cab motion
Number of data runs	8	8	8

In Phase I, the observations were taken, and entered, and all guidance and navigation computations were carried out on-line, in a real-time sequence typical of that phase of the mission. Phase I was restricted to the observation sequence immediately preceding the final velocity correction. In Phases II and III, observation error sets were processed off-line to allow an investigation of a number of complete return trajectories.

Phase I.- The Phase I study processed each of 12 observations as they were taken for the last velocity correction sequence, starting with the observation scheduled for 123.0 hours. The trajectory was divided into two parts: (1) the generation of the initial conditions at the 122.0 hour point, and (2) the study sequence covering the last 12 observations and the final return velocity correction. The initial conditions at the 122.0 hour point were obtained by starting the inbound trajectory at the moon-to-earth injection point (70.68 hr) with injection errors as previously described. A random

number generator was then used to generate instrument sighting errors based on a gaussian distribution with 10 seconds of arc standard deviation. The first 27 inbound observations were computed and processed, and both velocity corrections were simulated through a mission time of 122.0 hours, according to the observation and velocity correction schedule outlined in table II and illustrated in figure 13. The resulting errors in position and velocity obtained at the 122.0 hour point, shown in table III, constitute the initial condition errors used in all the subsequent Phase I data runs.

The real-time mission clock was initialized appropriately so that all observations were taken in a simulated real-time mission situation. Preliminary information that the observer had to enter prior to each observation included: observation number identification, star identification, and planet identification (moon or earth). After each observation of the celestial scene (as described previously), the actual and on-board trajectories were updated to the time of the observation. On the basis of these observations, the estimated velocity corrections were computed and then simulated. After the velocity corrections were executed, the resulting actual trajectories were integrated to the time of the reference trajectory vacuum perigee and to the actual vacuum perigee. Eight missions were completed in this manner.

Phase II.- The Phase II study used the actual observation set previously obtained from Phase I in a manner that would permit system performance analyses covering the entire inbound trajectory. The trajectory conditions were initialized at the moon-to-earth injection point identical to Phase I (table I). The 96 observation errors obtained in the Phase I data runs were then used by sequential cycling through the set to obtain all the observation errors required. These observations were processed, and all scheduled velocity corrections were simulated at the times given in table II. After the final velocity correction, the resulting trajectories were integrated to the time of the reference vacuum perigee and to the actual perigee time. Eight missions from injection to perigee were executed in this manner.

Phase III.- Phase III used observation data taken under dynamic conditions. The observer took observations while the moon simulator was moving with respect to the star background at 5 seconds of arc per second, considered a maximum rate for the midcourse phase. At the same time, the cab (fig. 10) was driven with a limit cycle of $\pm 2^\circ$ in all three axes at 0.08 Hz. Sixty-seven observations were taken off-line over a two-week period to reduce effects of fatigue. The resulting observation errors were used sequentially, as described for Phase II. After the final velocity correction, each resulting trajectory was computed to the time of the reference vacuum perigee and to the actual perigee time. Eight moon-to-earth return missions from injection to perigee were executed in this manner.

Theoretical Reference Data

To compute theoretical reference data to which the experimental data can be compared, variances of the injection errors are assumed known and normally distributed with zero mean. This statistical information in the form of

covariance matrices P and R allows the computation of the statistics of the entire ensemble of trajectories from one time to the next time of interest. The accuracy with which these covariance matrices represent the entire ensemble of trajectories depends upon the validity of the linear perturbation equations that are used to compute the transition matrix Φ; and the validity of the linear perturbation equations used is discussed in reference 1.

The 6 × 6 covariance matrix P (see box 4 of fig. 6, and appendix C) represents statistics of the error between the actual trajectory and the estimated trajectory, and is a fundamental part of the Kalman filter used in processing observations to obtain a better estimate of the position and velocity. As such, it is affected by the processing of each observation and depends on the assumed statistical performance, which in turn is based on the covariance matrix Q of sextant statistics, contained in the covariance matrix Q. The P matrix is partitioned as follows:

$$P = \begin{bmatrix} P_1 & P_2 \\ P_3 & P_4 \end{bmatrix} \tag{1}$$

and the rms magnitude of the position uncertainty of the estimated trajectory with respect to the actual trajectory $\tilde{r}_{rms}$ is computed as follows:

$$\tilde{r}_{rms} = [\text{trace } P_1]^{1/2} \tag{2}$$

The 6 × 6 covariance matrix R (see box 4 of fig. 6, and appendix C), which allows the computation of the statistics of the entire ensemble of actual trajectories with respect to the reference trajectory, is indirectly affected by the observation through the velocity correction. The R matrix is partitioned as follows:

$$R = \begin{bmatrix} R_1 & R_2 \\ R_3 & R_4 \end{bmatrix} \tag{3}$$

and the rms magnitude of the position uncertainty of the actual trajectory with respect to the reference trajectory $\hat{r}_{rms}$ is computed from the following:

$$\hat{r}_{rms} = [\text{trace } R_1]^{1/2} \tag{4}$$

The rms magnitude of the indicated velocity correction Δv_{rms} at any particular time along the trajectory depends on both P and R, and is computed from the 3 × 3 Δv matrix (see box 17 of fig. 6 and appendix C). The value of Δv_{rms} is used to evaluate the effect of sextant observation errors on the velocity correction, and is computed as follows:

$$\Delta v_{rms} = [\text{trace } \Delta v]^{1/2} \tag{5}$$

Values of $\tilde{r}_{rms}$, $\hat{r}_{rms}$, and Δv_{rms} were computed for sextants having errors with a standard deviation of 1, 10, and 50 seconds of arc. These values were computed with appropriate initial conditions for each of the three phases and were used as base line data. The experimental results are compared to this theoretical data in the discussion of the results. The standard deviation of the errors in the instrument is indicated in seconds of arc; for example, $\tilde{r}_{rms}(50)$ refers to data obtained assuming a sextant having errors with a standard deviation of 50 seconds of arc.

RESULTS

System guidance and navigation performance was evaluated on the basis of the following: (1) trajectory estimation accuracy by comparing the estimated trajectories with the actual trajectories; (2) velocity correction control by comparing the velocity correction magnitudes with theoretical reference data; (3) trajectory control by comparing the resulting actual trajectories with the on-board reference trajectory through actual trajectory vacuum perigee points, and by comparing data at the actual trajectory vacuum perigee with allowable limits.

Each research phase consisted of eight complete data runs. For graphical presentation the experimental results were reduced statistically to produce a composite trajectory envelope representing the standard deviation about the mean. This envelope, which is plotted for comparison with the theoretical reference data, consists of a "system performance 1 sigma upper boundary," and a "system performance 1 sigma lower boundary." The upper boundary curves were computed by adding the 1 sigma value computed for the eight data runs to the computed mean of the eight data runs, and the lower boundary curves were computed by subtracting the 1 sigma value from the mean.

In all the data runs using the experimental data, the Kalman filter equations assumed a standard deviation of the sextant error of 10 seconds of arc. The actual instrument data obtained were slightly better than those modeled in the Kalman filter. Consequently, a slightly mismatched situation resulted. Also, a specific, but typical, member of the ensemble was chosen to initialize the experimental data; this resulted in slightly degraded initial conditions for the experimental data as compared to the statistical conditions used in initializing the theoretical reference data.

Trajectory Estimation Accuracy

Trajectory estimation accuracy (1 sigma envelope) obtained in Phase I is illustrated in figure 14. The accuracy of the system performance estimation was generally equal to or better than that theoretically predicted for a system using an instrument with a standard deviation error of 10 seconds of arc. This can be seen by comparing the performance envelope with the theoretical

reference curve $\tilde{r}_{rms}(10)$. The system estimate after the last observation had an accuracy that an interpolation of the reference data indicates would result from processing observation data having 7-8 seconds-of-arc error. This trajectory estimation performance is considered acceptable because the resulting actual trajectories provide a safe reentry.

As previously mentioned, the initial conditions were obtained assuming a standard deviation error in the instrument of 10 seconds of arc and a statistical estimate of the instrument in the Kalman filter of 10 seconds of arc. Subsequent to the initialization point (fig. 14, point A), theoretical data were obtained for three reference cases: 1 second of arc, 10 seconds of arc, and 50 seconds of arc. For the 1 second case $\tilde{r}_{rms}(1)$, the subsequent data processing was sensitive to the more accurate measurements, as indicated in figure 14 by an immediate improvement in position estimation accuracy.

For $\tilde{r}_{rms}(10)$, as would be expected, there was no significant change in the estimation accuracy. When the standard deviation of the error in the instrument was changed to 50 seconds of arc $\tilde{r}_{rms}(50)$ a significant advantage of the Kalman filter was illustrated; the filter gives little weight to these degraded observations since the uncertainty of the estimated state (due to the higher initialization accuracy) is low compared to the new measurement uncertainty.

Phase II covered the complete mission, using the data of Phase I as previously described. As illustrated in figure 15, the system position estimation accuracy for this phase was very similar to that obtained for Phase I, and is considered quite adequate. An interpolation of the reference data indicated that performance of the system was equivalent to that indicated by the theoretical reference data for an instrument with about 5-6 seconds of error (standard deviation). In this phase, the theoretical reference data for $\tilde{r}_{rms}(50)$ had time to settle out and illustrate that performance of this type of instrument is unacceptable.

The Phase III data for the dynamic situation, where moving line-of-sight planet motion and cab-limit cycle motion are introduced, are illustrated in figure 16, which compares system estimation performance data through the complete in-bound trajectory with theoretical reference curves. The system estimation performance settled out around 20 kilometers of position estimation error. An interpolation of the theoretical reference curves indicated that this level of performance would result from processing observation data having 11-seconds-of-arc error, and thus would provide a safe, fixed-time-of-arrival reentry, which is consistent with theoretical predictions. The results are also consistent with the statistics of the observation error set obtained for this phase which, for the 67 observations that were taken, had a mean of 4.7 seconds of arc and a standard deviation of 8.6 seconds of arc giving an rms value of 9.8 seconds of arc. A comparison of statistical errors of the observation sets of Phases I and III indicates that the error increase due to the dynamics of Phase III is about 2.2 seconds of mean error (4.7 - 2.5), and that the standard deviation error increased by 2.7 seconds (8.6 - 5.9).

Velocity Correction

Table IV compares the velocity correction magnitudes obtained for all three phases with theoretical reference data. The comparison of velocity correction magnitudes of Phase I with theoretical reference data indicates satisfactory performance. There was a trend in Phase I for the velocity correction magnitude to be greater for the more accurate sextant models, as illustrated by a comparison of $\Delta v_{rms}(50)$ with $\Delta v_{rms}(1)$. This trend was an indirect result of the Kalman computation technique. An improvement in the knowledge of estimated position and velocity results in an increase in the magnitude of the velocity correction. When a series of corrections was made, as in Phases II and III, the sum of the velocity corrections showed that the more accurate instrument not only provided better actual position control (discussed below) but also minimized the expenditure of fuel, as one would expect.

The total velocity correction magnitudes obtained in Phases II and III (line 5, table IV) are consistent with the theoretical reference data. The magnitudes of Phase III, for example, are slightly larger than those obtained for a system having a theoretical 10-second standard deviation of the error in the instrument $\Delta v_{rms}(10)$, which is consistent with the position estimation performance discussed in the previous section.

Trajectory Control

Errors between the actual trajectory and the desired reference trajectory are shown for Phases I, II, and III, in figures 17, 18, and 19, respectively. Performance for all three study phases shows acceptable guidance and navigation. The increase in the upper error envelope boundary as the actual trajectory approaches the perigee point is to be expected because of the propagation of the uncertainties in the velocity correction. This upper error boundary still represents adequate systems performance; the actual trajectory errors from the reference trajectory result in a safe reentry state, as discussed in the following paragraph. Again, a comparison with theoretical data shows the resulting performance to be consistently better than that expected for a 10-second-of-error instrument.

Inasmuch as the altitude deviation at the actual perigee point is particularly critical and the errors in downrange and crossrange are also of interest in evaluating fixed time of arrival performance, the actual trajectory state is evaluated specifically at this point. The data are summarized in table V. Performance in position control at the actual perigee point was acceptable in all phases, as indicated by a comparison with the reference data and the allowable reentry corridor. The allowable reentry corridor data for this figure were obtained from references 12 and 13. Most of the position error at the actual perigee position is in the downrange direction and represents an error in fixed-time-of-arrival guidance of but a few seconds (the spacecraft velocity at this point in the downrange direction is approximately 11 km/sec).

Observer Comments on the Use of the Hand-Held Sextant

The observer was a qualified Air Force navigator (Capt.) with considerable experience with this type of instrument. He felt the hand-held sextant was operationally satisfactory for sightings of the type required in this experiment. The moon crater Tycho, used for the landmark reference, was easy to locate but there was some difficulty experienced by the observer in consistently determining the center accurately. He felt that actual sightings on the moon would be more difficult, mainly due to shadows of the craters shifting each day.

There were no significant problems during the static observations. The observer did find it desirable to introduce a small amount of instrument rotation motion during the observation. This motion produced a slow frequency motion of the star relative to the landmark with a magnitude as illustrated between points A and B of figure 12, and provided a more precise method of superimposing the star in the center of the landmark. During the dynamic measurements, the line-of-sight rates seemed very slow (5 seconds of arc per second). He felt that taking an observation was not any more difficult due to the moving line-of-sight variable than taking the observations under static conditions. However, the effects of the moving cab were significant, as this motion made it difficult to keep the star and the landmark superimposed. The motion of the cab coupled into the sextant and resulted in the same kind of star-landmark motion that was introduced by the observer in the static phase. However, this effect was far greater than desired. The observer attempted to reduce it by rotating the hand-held sextant in a direction opposite to the cab motion, but the resulting motion of the star and the landmark could not be reduced to less than that indicated by points C and D of figure 12. It is felt that this motion was the main source of error increase in the dynamic Phase III observations over those obtained from the static observations of Phases I and II.

The guidance and navigation performance obtained in this study were adequate, even though the cab motion used (2° at 0.08 Hz in all axes) was considerably in excess of that expected of an actual control system, and the coupling effects of this on the hand-held sextant were greater than desired. It is expected that under gravity-free conditions of space and isolation of the sextant from physical attachment to the shell of the vehicle, the error due to cab motion will actually be less than that experienced in this experiment.

Symbolic Computer Control and Display

The symbolic abbreviation computer control and display concept used in this study was identical to that reported in reference 9, except the panel configuration was modified for greater compatibility with cab installation requirements. Very satisfactory operational results were obtained through application of the symbolic-alphabetic abbreviation technique for entering and interpreting computer data. No errors were generated during input that were not detected and corrected by the observer, and there were no detectable display interpretation errors. The observer became familiar very rapidly with the abbreviations and the sequencing.

CONCLUSIONS

All three phases of this study further confirm through hardware simulation analysis that a system using a flight-qualified hand-held sextant and processing the observation data using statistical filter techniques have a basic potential of providing acceptable guidance and navigation for the midcourse phase. Position estimation was consistently good for all phases of this study, and the resulting velocity correction parameters were computed quite accurately from the position estimation data. The resulting capability of the system to guide the spacecraft to an acceptable reentry position and time was in all phases consistent with the requirements for a safe reentry. No anomalies or discontinuities were detected in the statistical filter processing of the hand-held sextant observation data. Operational results of using symbolic-alphabetic abbreviation techniques for computer control and display were very satisfactory.

The use of a hand-held sextant should result in significant system reliability advantages. Problems due to additional error sources, such as the effects of sighting through a window in the space environment, variations of the shadows on the moon, etc., will have to be considered before actual implementation of such a system in a spacecraft. However, the results of this study illustrate the basic capability of such a system to provide acceptable guidance and navigation information. Statistical filter theory processing of hand-held sextant data looks potentially good enough to warrant continued consideration for use in future manned spacecraft. The resulting hardware system configuration would offer very important advantages in simplicity and hence reliability.

Ames Research Center
National Aeronautics and Space Administration
Moffett Field, Calif., 94035, July 7, 1969

APPENDIX A

NONLINEAR EQUATIONS OF MOTION FOR TRAJECTORY CALCULATIONS

The equations of motion are derived under the following assumptions:

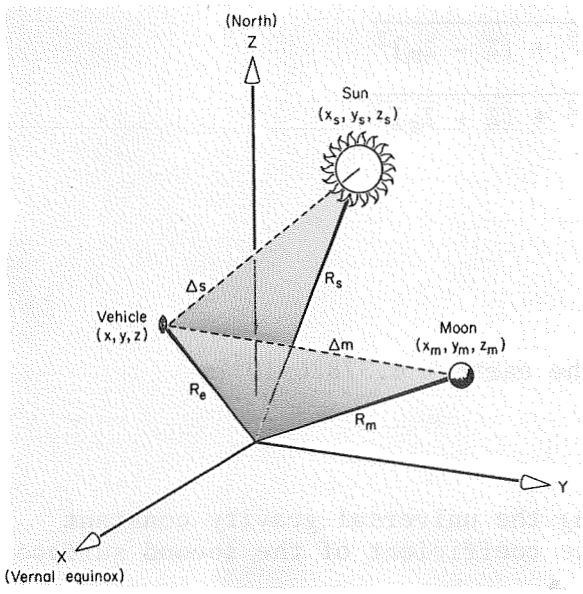

Sketch (a)

1. A restricted four-body system is sufficiently accurate.

2. The second harmonic term of the earth's gravitational field is sufficient.

3. The sun and moon are spherical and homogeneous.

The coordinate system is Cartesian and geocentric. The Z axis lies along the earth's polar axis, positive to the north. The X and Y axes lie in the equatorial plane with the positive X axis in the direction of the vernal equinox. The Y axis is oriented so as to form the right-handed orthogonal system shown in sketch (a).

The equations of motion, derived by methods given in reference 14, are:

$$\ddot{X} = -\frac{\mu_e X}{R_e^3}\left[1 + J\left(\frac{a}{R_e}\right)^2\left(1 - 5\frac{Z^2}{R_e^2}\right)\right] - \frac{\mu_m}{\Delta m^3}(X - X_m) - \frac{\mu_m X_m}{R_m^3} - \frac{\mu_s(X - X_s)}{\Delta s^3} - \frac{\mu_s X_s}{R_s^3} \tag{A1}$$

$$\ddot{Y} = -\frac{\mu_e Y}{R_e^3}\left[1 + J\left(\frac{a}{R_e}\right)^2\left(1 - 5\frac{Z^2}{R_e^2}\right)\right] - \frac{\mu_m}{\Delta m^3}(Y - Y_m) - \frac{\mu_m Y_m}{R_m} - \frac{\mu_s(Y - Y_s)}{\Delta s^3} - \frac{\mu_s Z_s}{R_s^3} \tag{A2}$$

$$\ddot{Z} = -\frac{\mu_e Z}{R_e^3}\left[1 + J\left(\frac{a}{R_e}\right)^2\left(3 - 5\frac{Z^2}{R_e^2}\right)\right] - \frac{\mu_m(Z - Z_m)}{\Delta m^3} - \frac{\mu_m Z_m}{R_m^3} - \frac{\mu_s(Z - Z_s)}{\Delta s^3} - \frac{\mu_s Z_s}{R_s^3} \tag{A3}$$

where

$$R_e = \sqrt{X^2 + Y^2 + Z^2}$$

$$R_m = \sqrt{X_m^2 + Y_m^2 + Z_m^2}$$

$$R_s = \sqrt{X_s^2 + Y_s^2 + Z_s^2}$$

$$\Delta m = \sqrt{(X - X_m)^2 + (Y - Y_m)^2 + (Z - Z_m)^2}$$

$$\Delta s = \sqrt{(X - X_s)^2 + (Y - Y_s)^2 + (Z - Z_s)^2}$$

$$\mu_e = 3.986135 \times 10^{14} \text{ m}^3/\text{sec}^2$$

$$\mu_m = 4.89820 \times 10^{12} \text{ m}^3/\text{sec}^2$$

$$\mu_s = 1.3253 \times 10^{20} \text{ m}^3/\text{sec}^2$$

a = equatorial radius of the earth = 6.37826×10^6 m

$$J = 1.6246 \times 10^{-3}$$

The μ values are computed by multiplying the universal gravity constant times the mass of the body, and J is the coefficient of the second surface harmonic of the earth's potential field.

The terms involving only distances between the earth and moon, or earth and sun, such as $\mu_m X_m / R_m^3$, account for the accelerations of the coordinate system with respect to inertial space.

The position of the sun and moon are obtained by interpolation of data from magnetic tape ephemerides. Within the sphere of influence of the moon, a lunar radius of 66,000 km, the origin of coordinates is translated to the center of the moon. Since no rotation is performed, the definitions of perturbations from the reference (see appendix B) remain the same.

APPENDIX B

CALCULATION OF TRANSITION MATRICES

The transition matrices used in the navigation system are obtained by solving linear differential equations that represent perturbations of the actual trajectory from the reference. Derivation of these perturbation differential equations is outlined below.

The nonlinear equations of motion given in appendix A can be written in the form:

$$\left.\begin{aligned} \ddot{X} &= F_1(X,Y,Z,t) \\ \ddot{Y} &= F_2(X,Y,Z,t) \\ \ddot{Z} &= F_3(X,Y,Z,t) \end{aligned}\right\} \tag{B1}$$

It is desired to find linear differential equations for small deviations from the reference. These equations may be found by expanding equations (B1) about the reference trajectory in a Taylor series and dropping all terms except the first order.

$$\left.\begin{aligned} \delta\ddot{X} &= \frac{\partial F_1}{\partial X}\delta X + \frac{\partial F_1}{\partial Y}\delta Y + \frac{\partial F_1}{\partial Z}\delta Z \\ \delta\ddot{Y} &= \frac{\partial F_2}{\partial X}\delta X + \frac{\partial F_2}{\partial Y}\delta Y + \frac{\partial F_2}{\partial Z}\delta Z \\ \delta\ddot{Z} &= \frac{\partial F_3}{\partial X}\delta X + \frac{\partial F_3}{\partial Y}\delta Y + \frac{\partial F_3}{\partial Z}\delta Z \end{aligned}\right\} \tag{B2}$$

It is convenient to deal with systems of linear differential equations in multiple variables in matrix form. For this purpose, it is generally desirable to reduce the system to a set of first-order equations as follows. Define

$$\left.\begin{aligned} x_1 &= \delta X & x_4 &= \delta\dot{X} \\ x_2 &= \delta Y & x_5 &= \delta\dot{Y} \\ x_3 &= \delta Z & x_6 &= \delta\dot{Z} \end{aligned}\right\} \tag{B3}$$

Then the system of perturbation equations can be written in matrix form as

$$\frac{dx}{dt} = F(t)x \tag{B4}$$

where F is a 6×6 matrix of coefficients and x is a 6×1 column vector of the x_i defined above. From equations (B2) and (B3), equation (B4) can be written as

$$\begin{bmatrix} \dot{x}_1 \\ \dot{x}_2 \\ \dot{x}_3 \\ \dot{x}_4 \\ \dot{x}_5 \\ \dot{x}_6 \end{bmatrix} = \begin{bmatrix} 0 & 0 & 0 & 1 & 0 & 0 \\ 0 & 0 & 0 & 0 & 1 & 0 \\ 0 & 0 & 0 & 0 & 0 & 1 \\ \frac{\partial F_1}{\partial X} & \frac{\partial F_1}{\partial Y} & \frac{\partial F_1}{\partial Z} & 0 & 0 & 0 \\ \frac{\partial F_2}{\partial X} & \frac{\partial F_2}{\partial Y} & \frac{\partial F_2}{\partial Z} & 0 & 0 & 0 \\ \frac{\partial F_3}{\partial X} & \frac{\partial F_3}{\partial Y} & \frac{\partial F_3}{\partial Z} & 0 & 0 & 0 \end{bmatrix} \begin{bmatrix} x_1 \\ x_2 \\ x_3 \\ x_4 \\ x_5 \\ x_6 \end{bmatrix} \tag{B5}$$

Consider any system of homogeneous linear first-order differential equations written in matrix form

$$\frac{dx}{dt} = \mathfrak{J}(t)x \tag{B6}$$

where $\mathfrak{J}$ is an $n \times n$ matrix of time variant coefficients and x is an $n \times 1$ column vector of dependent variables. It is shown in reference 13 that if U is a nonsingular matrix having n columns of n linearly independent solutions of (B6), then U (defined as a fundamental matrix) is a solution of

$$\frac{dU}{dt} = \mathfrak{J}(t)U \tag{B7}$$

where $U(t_o)$ is a constant matrix. As a special case, Φ is defined as being the U obtained when $U(t_o)$ is the unit matrix. Thus Φ can be obtained one column at a time if equation (B6) is solved n times, each with a different member of $x(t_o)$ set equal to unity and all the other members set equal to zero. Once Φ is obtained the solution of $x(t)$ for any given set of initial conditions x_o is given by

$$x(t) = \Phi(t)x_o \tag{B8}$$

The matrix $\Phi(t)$ represents the "transition in the states of the system of equations between time t_o and t and may be written as $\Phi(t,t_o)$ to indicate this fact. If equation (B5) is solved in this manner, the resulting transition matrix relates deviations from the reference trajectory at time t to the initial deviations at time t_o. The transition matrix $\Phi(t_2,t_1)$ between any two times on the reference trajectory may be calculated in the same manner as $\Phi(t,t_o)$.

The calculation is performed on the SDS 920 computer by solving six sets of perturbation equations, each with a unit initial condition on one of the x_i, between succeeding observations. After each observation, the initial conditions are reset, to unity or zero, and the computation is carried out until the next observation. Additional details of this development may be obtained from reference 1.

APPENDIX C

GUIDANCE, NAVIGATION, AND STATISTICAL DATA COMPUTATIONS

LINEAR PREDICTION

The linear prediction used is covered in detail in reference 1. It assumes that small deviations of the state at time t_k can be obtained from a linear combination of the deviations at time t_{k-1}. In particular, when dealing with the deviations $\tilde{x}(t_{k-1})$ and $x(t_{k-1})$, the relationships may be written in matrix form as follows:

$$\tilde{x}(t_k) = \Phi(t_k,t_{k-1})\tilde{x}(t_{k-1}) \tag{C1}$$

$$x(t_k) = \Phi(t_k,t_{k-1})x(t_{k-1}) \tag{C2}$$

where $\Phi(t_k,t_{k-1})$ is the transition matrix from time t_{k-1} to time t_k. Substituting (C1) into the definition of the covariance matrix of estimation error $P(t_k)$ where

$$P(t_k) = E[\tilde{x}(t_k)\tilde{x}^T(t_k)] \tag{C3}$$

yields the following equation relating $P(t_{k-1})$ to $P(t_k)$:

$$P(t_k) = \Phi(t_k,t_{k-1})P(t_{k-1})\Phi^T(t_k,t_{k-1}) \tag{C4}$$

Similarly, substituting (C2) into the definition of the covariance matrix of the deviations between the actual and the reference states $R(t_k)$ where

$$R(t_k) = E[x(t_k)x^T(t_k)] \tag{C5}$$

yields the following equation relating $R(t_{k-1})$ to $R(t_k)$:

$$R(t_k) = \Phi(t_k,t_{k-1})R(t_{k-1})\Phi^T(t_k,t_{k-1}) \tag{C6}$$

Thus, the updating operation consists of computing equations (C4) and (C6).

H MATRIX

The H matrix is computed from the reference state values in the form

$$H(t_k) = \left(\frac{\partial y}{\partial X}\ \frac{\partial y}{\partial Y}\ \frac{\partial y}{\partial Z}\right) \tag{C7}$$

where the partial derivatives of the sextant angle y are found from an expression for y in terms of position components (X, Y, Z) and the unit vector to the selected star.

KALMAN WEIGHTING MATRIX

The Kalman weighting matrix K at time t_k is computed for this application in the form given in reference 1, as follows:

$$K(t_k) = P(t_k)H^T(t_k)[H(t_k)P(t_k)H^T(t_k) + Q]^{-1} \tag{C8}$$

where Q is a covariance matrix of the observational errors. For this particular case Q is given as

$$Q = [\sigma^2] \tag{C9}$$

where σ^2 is the variance of the error in the instrument in seconds of arc assuming zero mean error.

COVARIANCE MATRIX OF THE ESTIMATION ERROR P

The value of the covariance matrix of estimation error after a sextant observation $P'(t_k)$ is computed as follows:

$$P'(t_k) = P(t_k) - K(t_k)H(t_k)P(t_k) \tag{C10}$$

This computation reflects the change in the covariance matrix of estimation errors P due to the observation just processed, and $P'(t_k)$ now becomes the updated $P(t_k)$ and $P(t_k)$ is then stored.

THE END-POINT STATE PREDICTION MATRIX A

A prediction matrix $A(t_e,t_k)$, which predicts the end-point state from the present state, is computed from

$$A(t_e,t_k) = A(t_e,t_{k-1})\Phi(t_k,t_{k-1})^{-1} \tag{C11}$$

An initial prediction matrix $A(t_e,t_o)$ is required to start the above computation and is determined prior to the initialization of the program. To obtain this matrix, the system was commanded, prior to any actual data runs, to run from the reference trajectory injection point at t_o to the end-point t_e without observations or velocity corrections. This resulted in a transition matrix $\Phi(t_e,t_o)$, which was also the desired initial prediction matrix $A(t_e,t_o)$. Updating of the prediction matrix at each observation according to equation (C11) required finding $\Phi(t_k,t_{k-1})^{-1}$ from $\Phi(t_k,t_{k-1})$. Because

$\Phi(t_k,t_{k-1})$ is a symplectic matrix, it is invertable merely by rearranging terms and changing signs. Thus, if $\Phi(t_k,t_{k-1})$ is partitioned into 3×3 submatrices

$$\Phi(t_k,t_{k-1}) = \begin{bmatrix} \Phi_1 & \Phi_2 \\ \Phi_3 & \Phi_4 \end{bmatrix} \tag{C12}$$

then

$$\Phi(t_k,t_{k-1})^{-1} = \begin{bmatrix} \Phi_4^T & -\Phi_2^T \\ -\Phi_3^T & \Phi_1 \end{bmatrix} \tag{C13}$$

INDICATED VELOCITY CORRECTION ΔV_G

With the difference between the estimated and reference states given by $\hat{x}$ and the updated prediction matrix from equation (C11) the indicated velocity correction ΔV_G to be gained is computed from

$$\begin{bmatrix} 0 \\ 0 \\ 0 \\ \Delta V_{GX} \\ \Delta V_{GY} \\ \Delta V_{GZ} \end{bmatrix} = \begin{bmatrix} 0 \\ \\ . \ . \ . \\ \\ \Delta V_G \\ \\ \end{bmatrix} = G\hat{x} \tag{C14}$$

where G is given by

$$G = \left[\begin{array}{ccc:c} & 0 & & 0 \\ \hdashline A_2^{-1}(t_e,t_k) & & A_1(t_e,t_k) & I \end{array}\right] \tag{C15}$$

and $A_1(t_e,t_k)$ and $A_2(t_e,t_k)$ are 3×3 submatrices resulting from the partitioning of $A(t_e,t_k)$.

The magnitude of ΔV_G is

$$|\Delta V_G| = (\Delta V_G{}^T \Delta V_G)^{1/2} \tag{C16}$$

COVARIANCE MATRIX ΔV

The statistics of the indicated velocity correction are determined from a covariance matrix ΔV, which is computed from

$$\begin{aligned} \Delta V &= E[\Delta V_G \ \Delta V_G{}^T] \\ &= GE[\hat{x}\hat{x}^T]G^T \end{aligned} \tag{C17}$$

In reference 1, it is shown that

$$E[\hat{x}\hat{x}^T] = R - P \tag{C18}$$

so that the actual computation is

$$\Delta V = G[R - P]G^T \tag{C19}$$

COVARIANCE MATRIX R

The covariance matrix R of the errors between the actual and the estimated states must be corrected to reflect the effects of the velocity correction maneuver: The required computation, developed in detail in reference 1, is as follows:

$$R' = (I + G)(R - P)(I + G)^T + P$$

where R' is the updated R matrix and replaces R.

REFERENCES

1. McLean, John D.; Schmidt, Stanley F.; and McGee, Leonard A.: Optimal Filtering and Linear Prediction Applied to a Midcourse Navigation System for the Circumlunar Mission. NASA TN D-1208, 1962.

2. Smith, Gerald L.; Schmidt, Stanley F.; McGee, Leonard A.: Application of Statistical Filter Theory to the Optimal Estimation of Position and Velocity On Board a Circumlunar Vehicle. NASA TR R-135, 1962.

3. Smith, Gerald L.: Multivariable Linear Filter Theory Applied to Space Vehicle Guidance. J. Soc. Industrial and Appl. Math., ser. A - Control, vol. 2, no. 1, 1964, pp. 19-32.

4. Lampkin, Bedford A.; and Randle, Robert J.: Investigation of a Manual Sextant-Sighting Task in the Ames Midcourse Navigation and Guidance Simulator. NASA TN D-2844, 1965.

5. Lampkin, Bedford A.: Sextant Sighting Performance for Space Navigation Using Simulated and Real Celestial Targets, Navigation: 1. Inst. Navigation, vol. 12, Winter 1965-1966, pp. 312-320.

6. Smith, Donald W.: The Hand-Held Sextant - Results From Gemini XII and Flight Simulator Experiments. J. Spacecraft and Rockets, vol. 5, June 1968, pp. 655-662.

7. Lampkin, Bedford A.; and Smith, Donald W.: A Hand-Held Sextant Qualified for Space Flight. NASA TN D-4585, 1968.

8. Smith, Donald W.; and Lampkin, Bedford A.: Sextant Sighting Measurements From On Board the Gemini VII Spacecraft. NASA TN D-4952, 1968.

9. Christensen, Jay V.; and Kipping, E. David: Midcourse Navigation Using Statistical Filter Theory, A Manual Theodolite and Symbolic Computer Control. NASA TN D-3875, 1967.

10. Mersman, William A.: Self-Starting Multistop Methods for the Numerical Integration of Ordinary Differential Equations. NASA TN D-2936, 1965.

11. Christensen, Jay V.: Digital Simulation Techniques for Lunar Midcourse Guidance and Navigation Computer Systems Research. Supplement to IEEE Trans. Aerospace and Electronics Sys., vol. AES-2, July 1966, pp. 832-836.

12. Duncan, Robert C.: Apollo Navigation, Guidance and Control. Apollo Lunar Landing Mission Symposium, NASA Manned Spacecraft Center, Houston, Texas, vol. I, June 25-27, 1966, pp. 83-130.

13. Frank, M. P.: Transearth Injection Through Reentry. Apollo Lunar Landing Mission Symposium. NASA Manned Spacecraft Center, Houston, Texas, vol. II, June 25-27, 1966, pp. 313-325.

14. Moulton, Forest Ray: An Introduction to Celestial Mechanics. Second ed., The MacMillan Co., 1959.

15. Stone, C. R.; Johnson, Charles W.; Smith, Fred B.; Lee, E. Bruce; and Harvey, Charles A.: Time-Optimal Control of Linear Systems. Aero. Document R-ED6134, Minneapolis-Honeywell Regulator Co., Sept. 1, 1959.

TABLE I.- INITIAL CONDITION ERRORS AT THE TRANSEARTH INJECTION POINT
[Perilune: 70.68 hr]

Parameter	Initial condition errors
X	-0.588 km
Y	-.304 km
Z	1.254 km
$\dot{X}$	.001359 km/sec
$\dot{Y}$	.000949 km/sec
$\dot{Z}$	.000449 km/sec

TABLE II.- OBSERVATION AND VELOCITY CORRECTION SCHEDULE

Mission time, hr	Mission function	Observed body
70.68	Transearth injection time	
71.0	Observation	Moon
71.5		
72.0		
72.5		
73.0		
73.5		
74.0		
74.5		
75.0		
75.5		
76.0		Earth
76.5		
77.0		
77.5		
78.0		
78.5		
79.0		
79.5		
80.0		
80.5		
81.0	1st return velocity correction	
109.0	Observation	Moon
110.0		Moon
111.0		Earth
112.0		
113.0		
114.0		
115.0		
116.0	2nd return velocity correction	
123.0	Observation	Moon
124.0		
125.0		
126.0		Earth
127.0		
128.0		
129.0		
130.0		
131.0		
132.0		Moon
133.0		
134.0		
135.0	Final return velocity correction	
144.874633	Time of reference perigee (aim point)	

TABLE III.- INITIAL CONDITION ERRORS AT 122.0 HOURS
AS USED IN PHASE I

Parameter	Error
X	72.594 km
Y	1.855 km
Z	-19.889 km
$\dot{X}$	-0.000648 km/sec
$\dot{Y}$	.000328 km/sec
$\dot{Z}$	.000276 km/sec

TABLE IV.- VELOCITY CORRECTION MAGNITUDES, m/sec

	Phase I data	Phase I $\Delta v_{rms}(1)$	Phase I $\Delta v_{rms}(10)$	Phase I $\Delta v_{rms}(50)$	Phase II data	Phase III data	Phase II and III $\Delta v_{rms}(1)$	Phase II and III $\Delta v_{rms}(10)$	Phase II and III $\Delta v_{rms}(50)$
First return velocity correction	---	---	---	---	2.87 ±.97	3.08 ±.24	3.35	3.34	3.18
Second return velocity correction	---	---	---	---	1.26 ±.37	1.56 ±.76	.11	.86	2.42
Third return velocity correction	0.49 ±.23	1.07	0.81	0.27	.37 ±.27	.62 ±.30	.10	.81	2.58
Total velocity correction	---	---	---	---	4.19 ±.53	5.28 ±.95	3.56	5.01	8.18

NOTE: Plus and minus data are standard deviation data.

TABLE V.- POSITIONAL ERROR (ACTUAL-REFERENCE) AT ACTUAL PERIGEE, km

Parameter	Phase I data	$\hat{r}_{rms}(1)$	$\hat{r}_{rms}(10)$	$\hat{r}_{rms}(50)$	Phase II data	Phase III data	$\hat{r}_{rms}(1)$	$\hat{r}_{rms}(10)$	$\hat{r}_{rms}(50)$	Maximum allowable reentry corridor
Altitude	1.9 ±1.1	±0.3	±2.1	±3.0	1.9 ±1.1	2.8 ±1.1	±0.2	±2.3	±5.8	±21.0
Crossrange	.3 ±.1	±.1	±.3	±.4	.2 ±.1	.4 ±.2	±0	±.3	±.7	±355.0
Downrange	-38.7 ±38.8	±11.1	±77.0	±113.6	10.3 ±38.9	8.9 ±50.9	±8.4	±76.9	±280.8	±806.0

Single signed data are mean of the data and the plus and minus data are standard deviation data for the 8 missions that comprised each data phase.

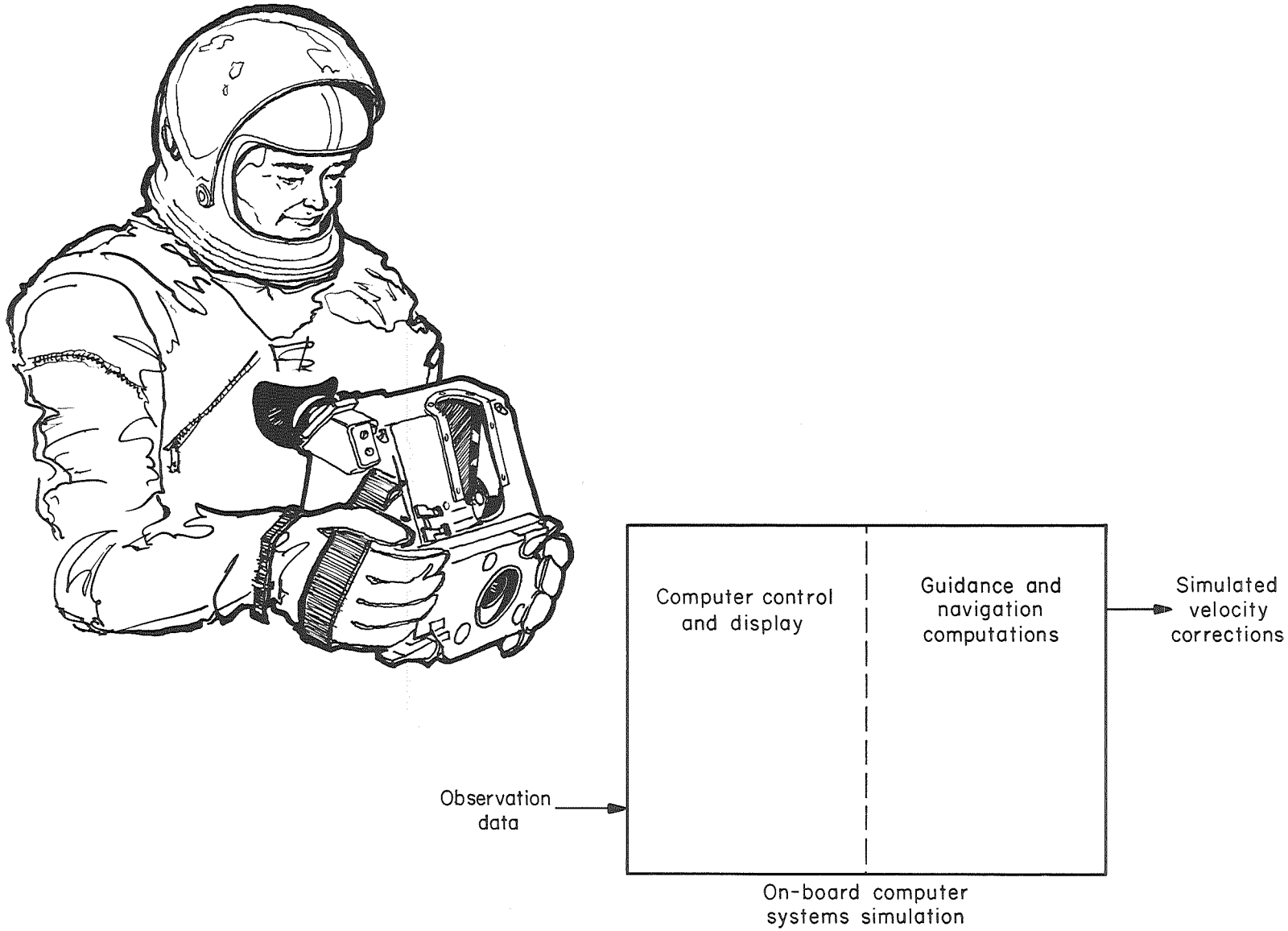

Figure 1.- On-board hardware-computational system configuration.

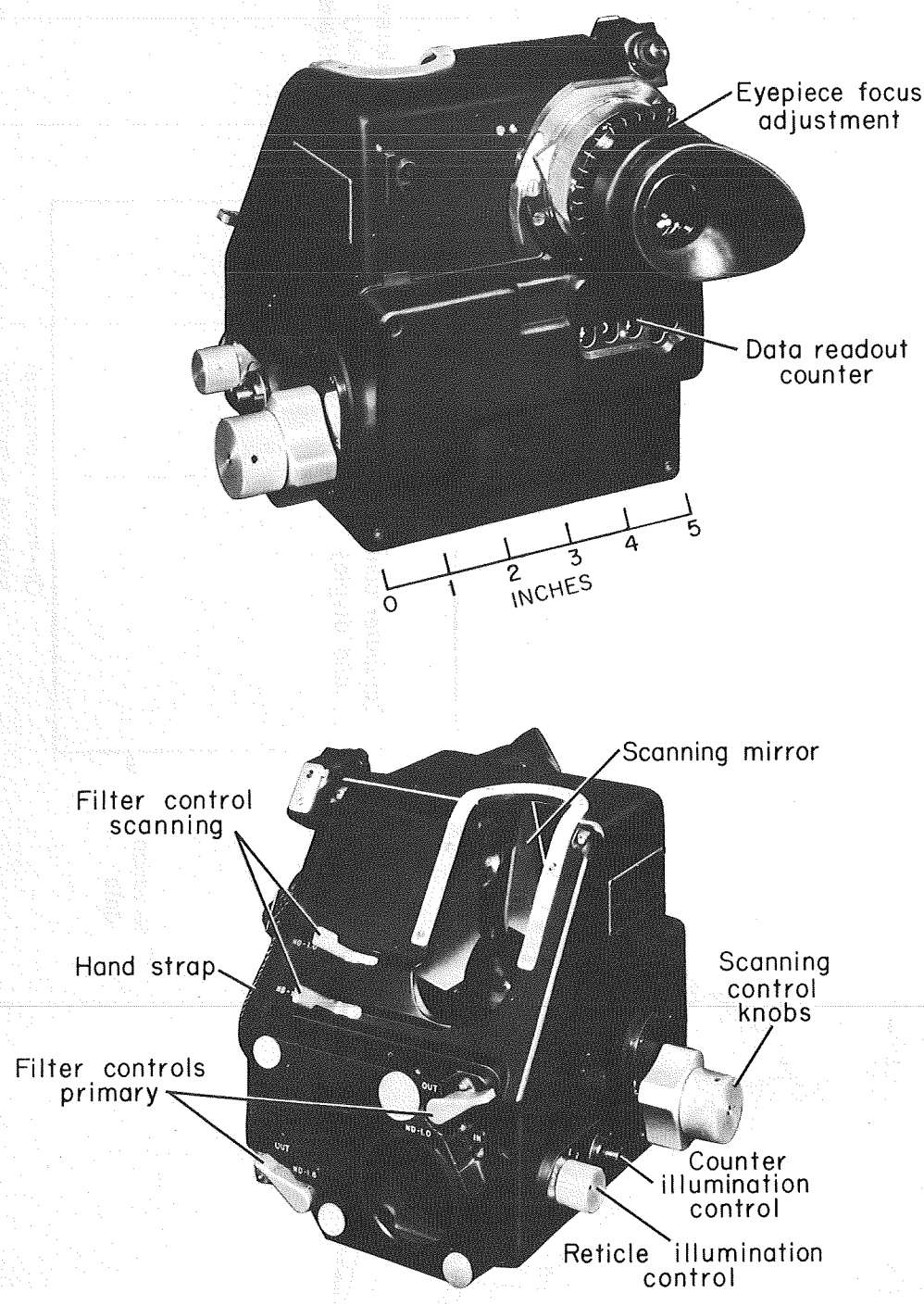

Figure 2.- Sextant configuration and operating controls.

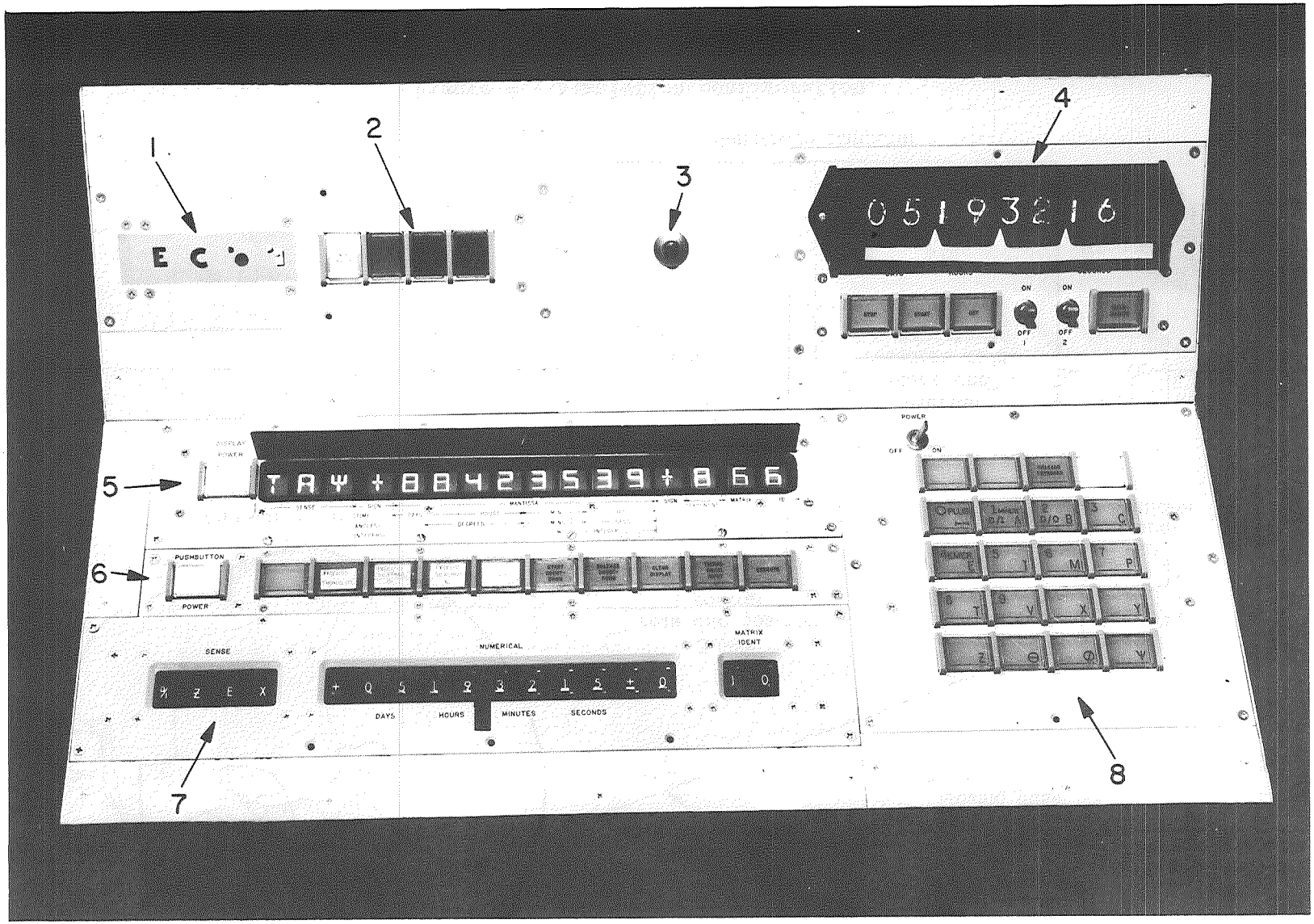

A-35114.1

Figure 3.- Lunar midcourse computer control and display panel.

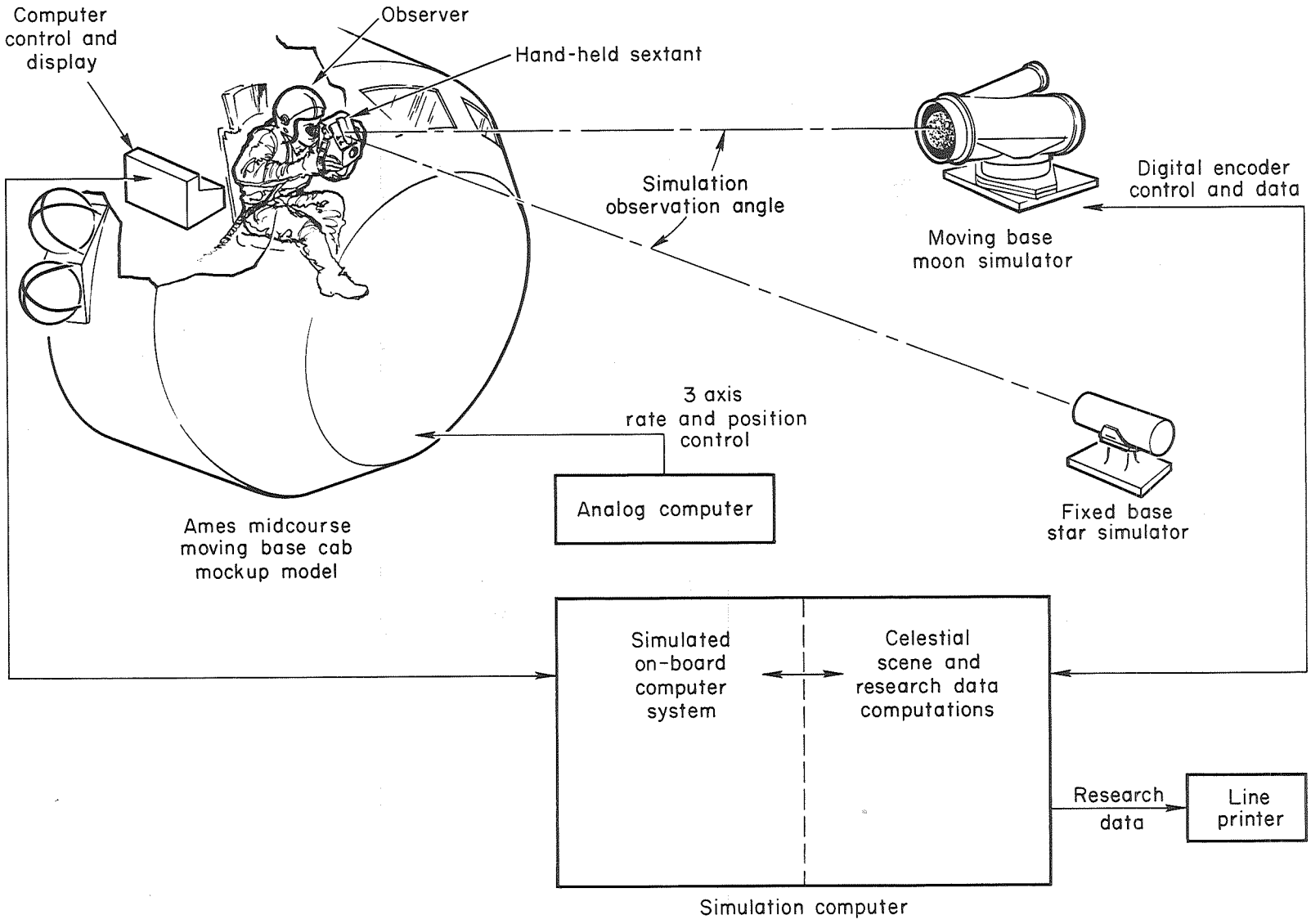

Figure 4.- Simulation configuration.

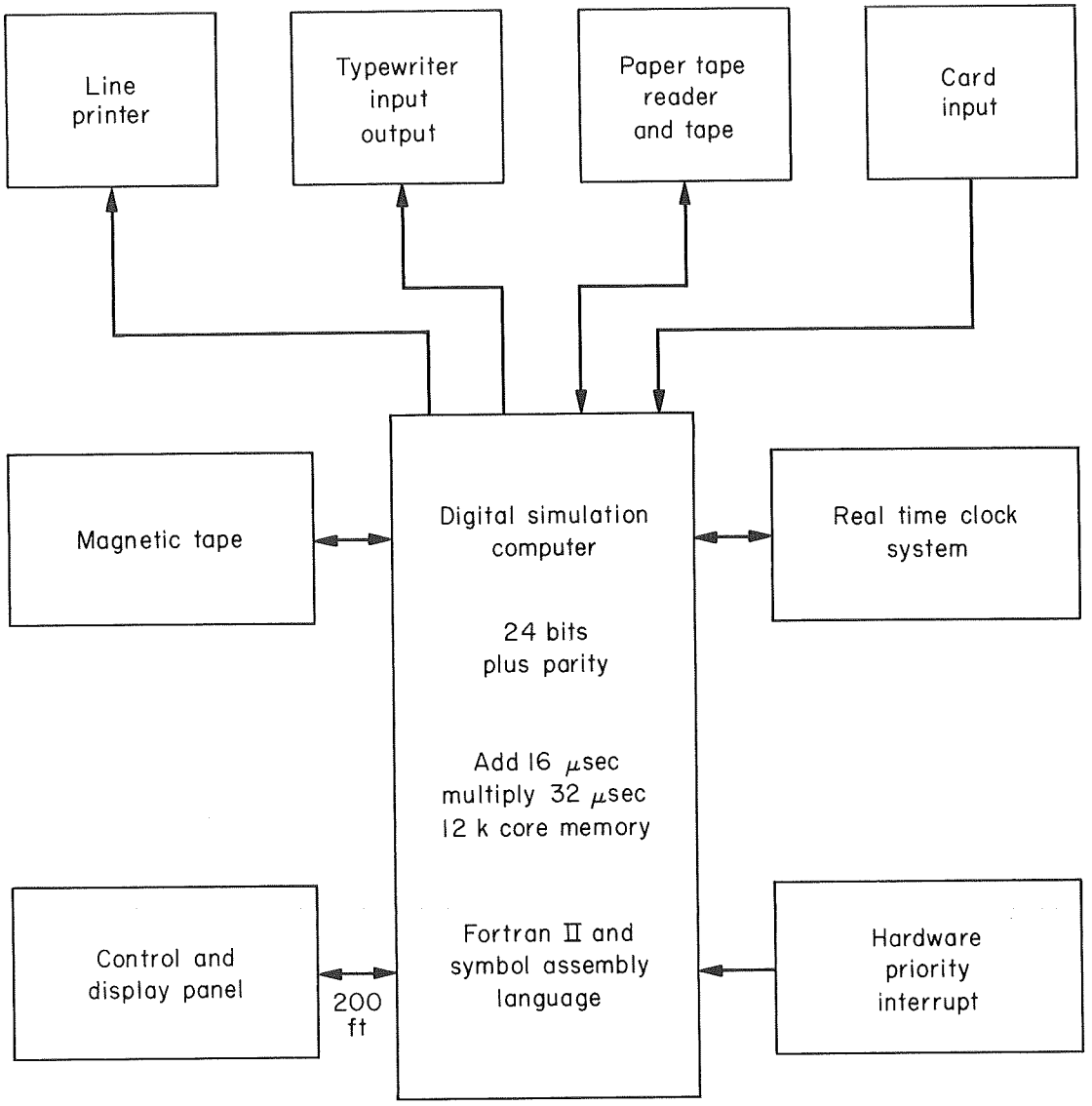

Figure 5.- Digital computer simulation configuration.

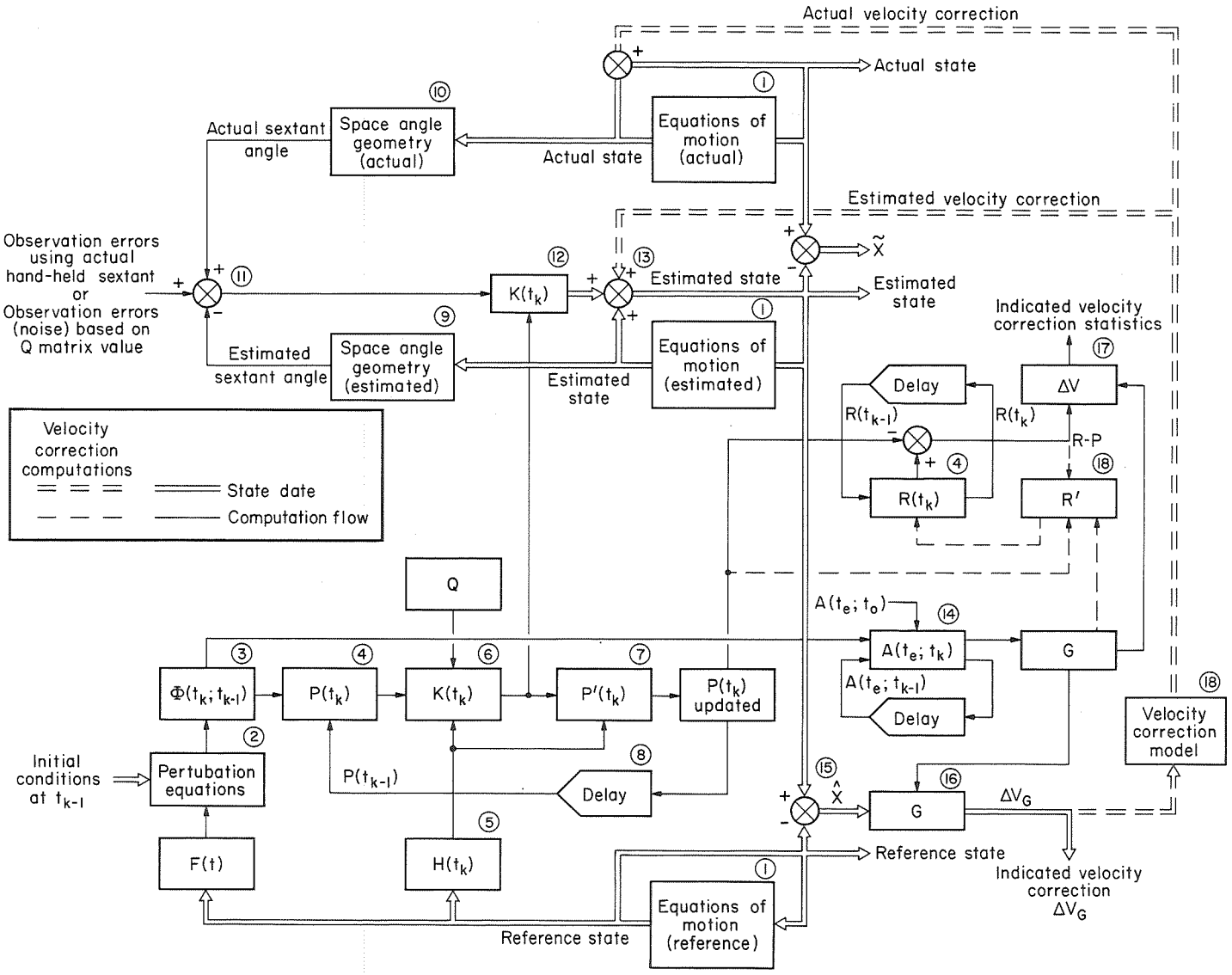

Figure 6.- Block diagram of digital computations.

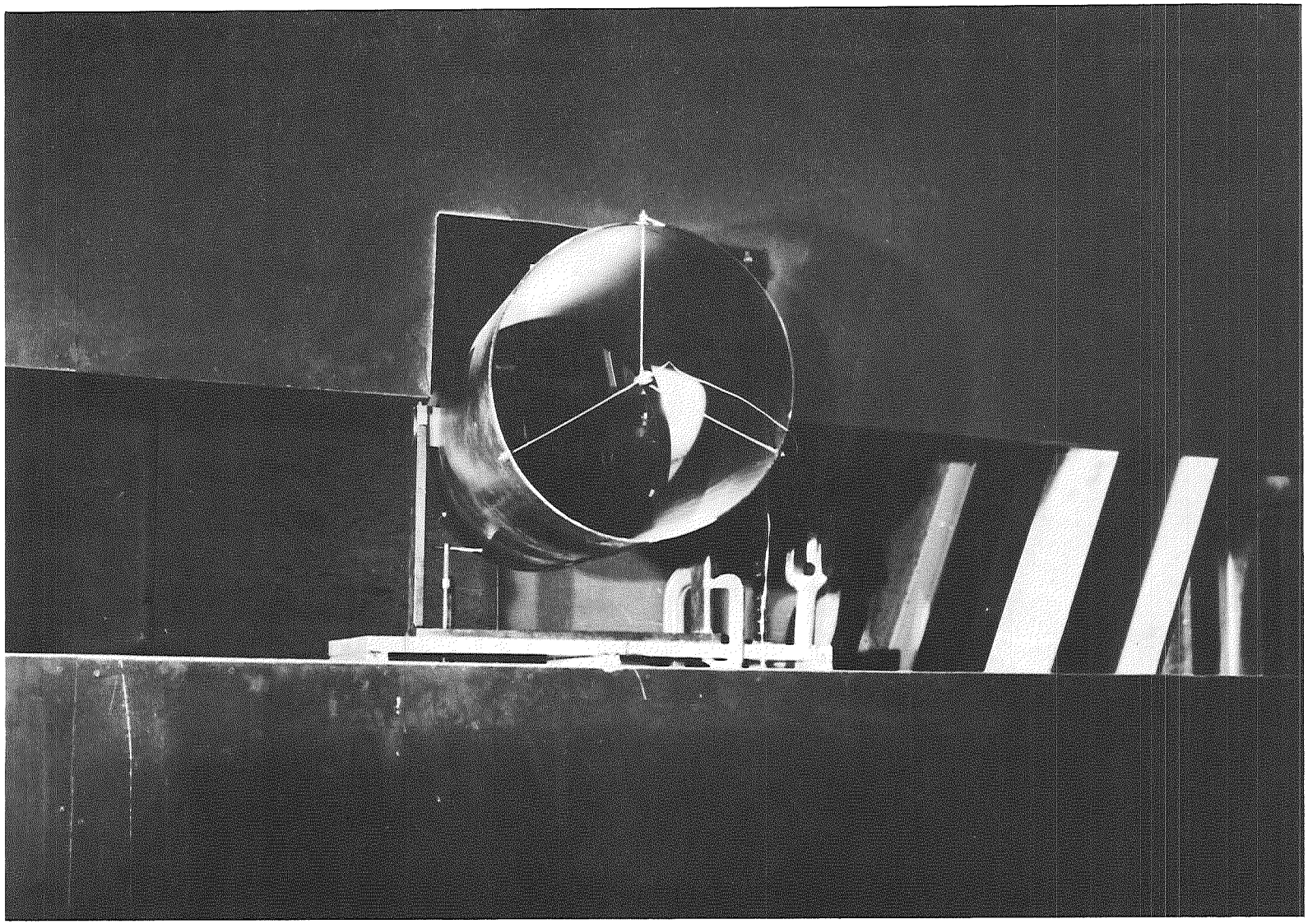

A-40576

Figure 7.- Star simulator.

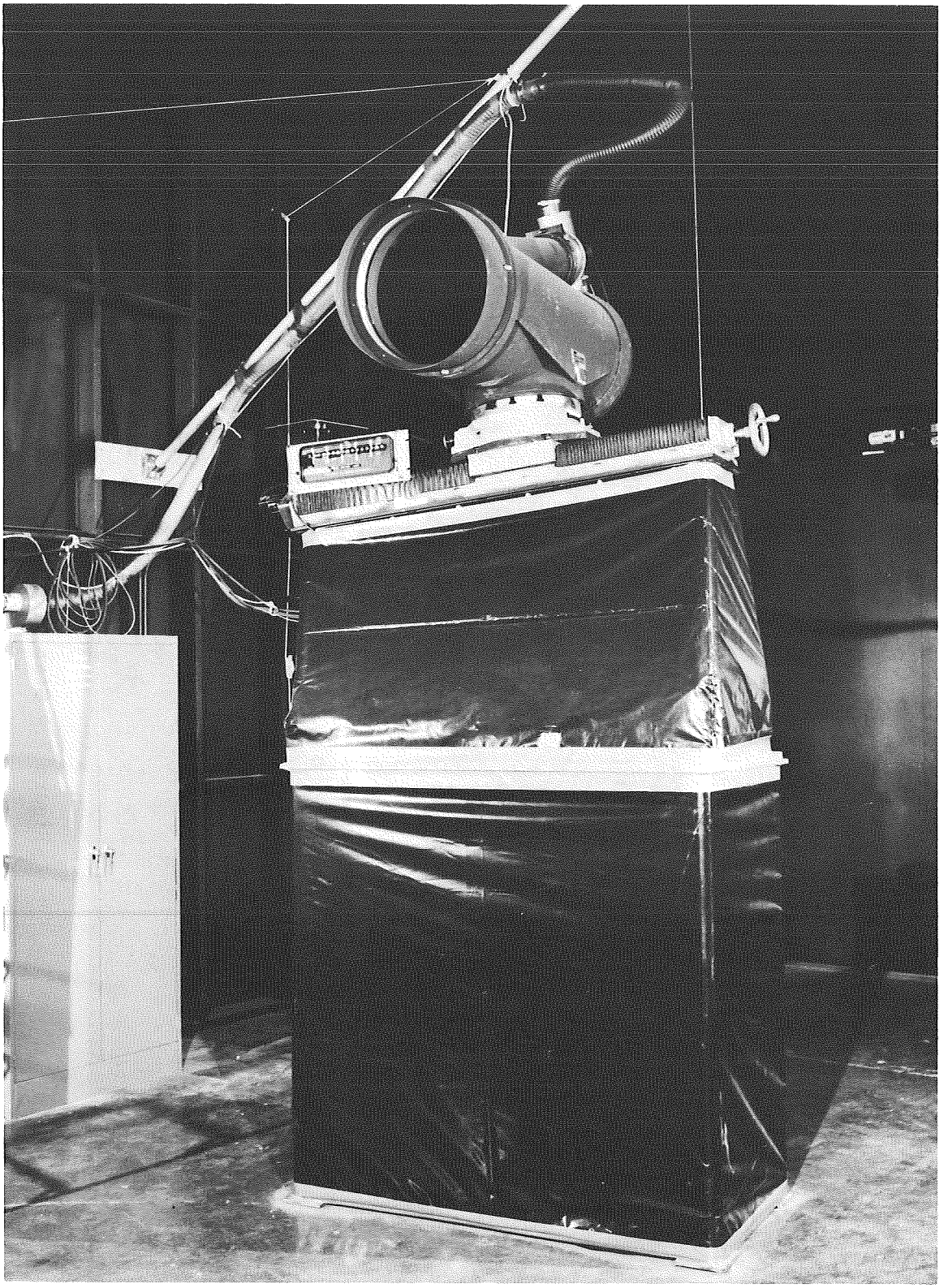

A-40577

Figure 8.- Moon simulator.

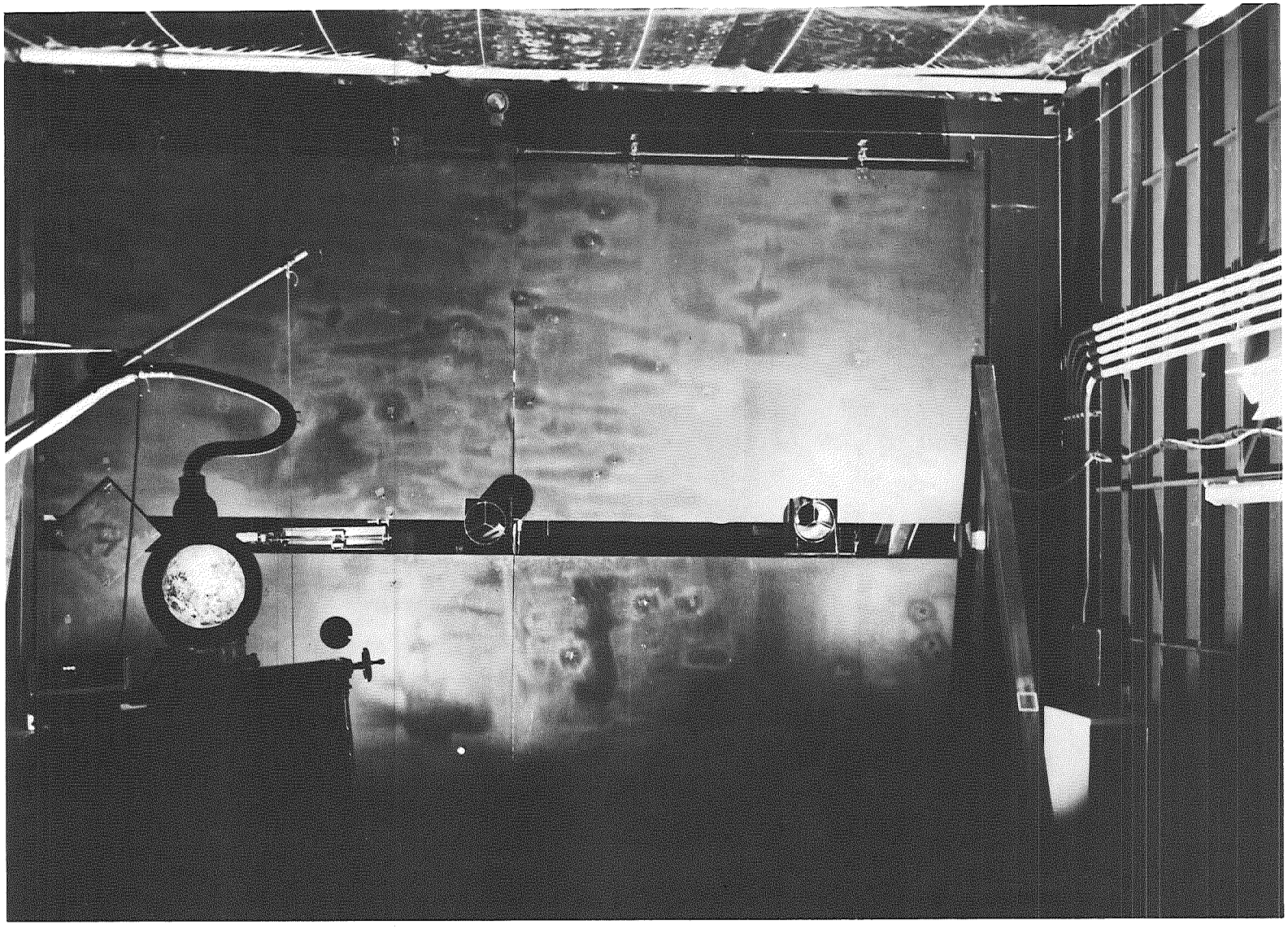

A-40579

Figure 9.- Simulated celestial scene as viewed from the observer's station in the cab.

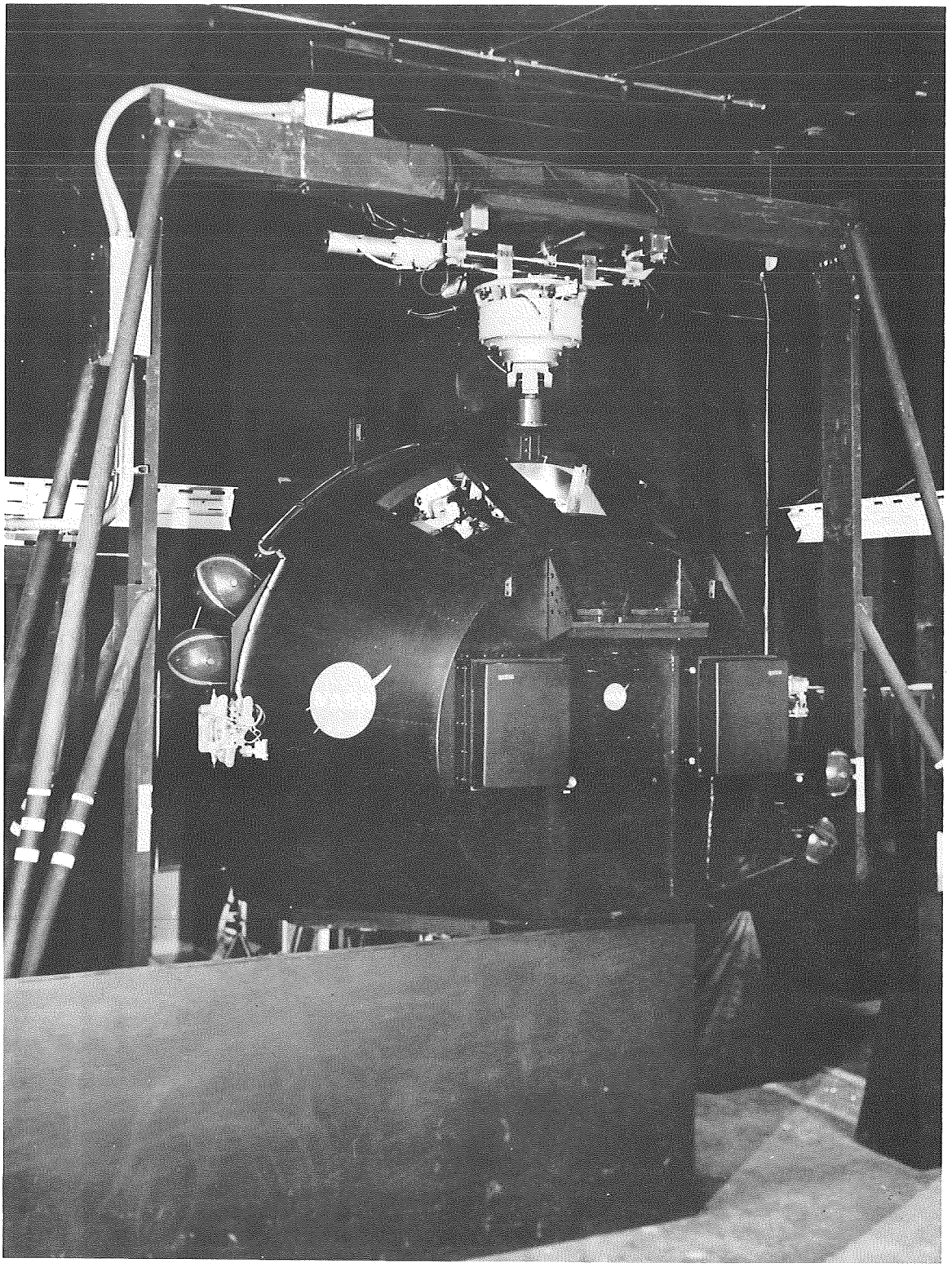

A-37370

Figure 10.- Lunar midcourse spacecraft cab simulator.

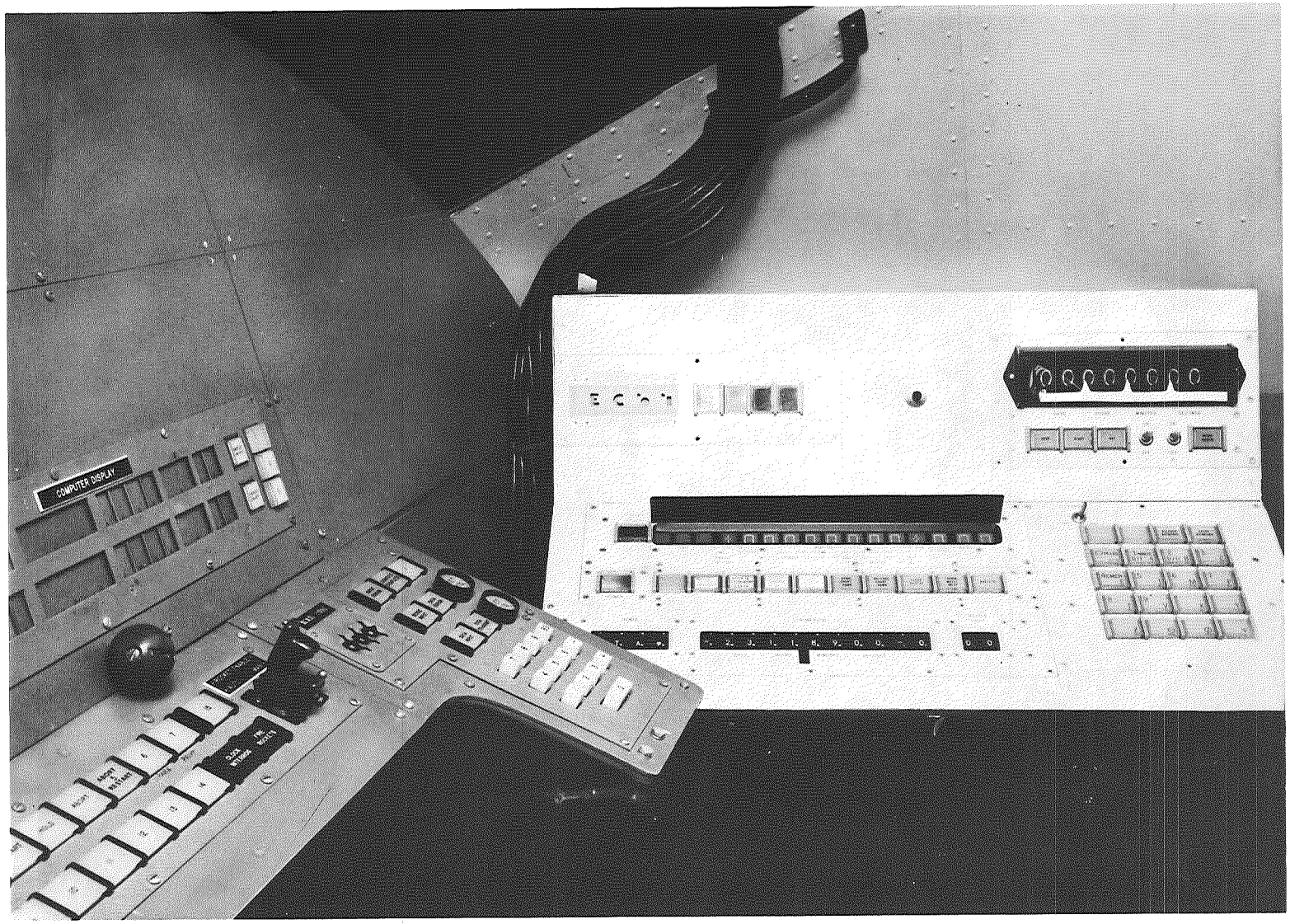

A-40578.1

Figure 11.- Computer control and display panel installed in the cab.

Figure 12.- Moon photograph.

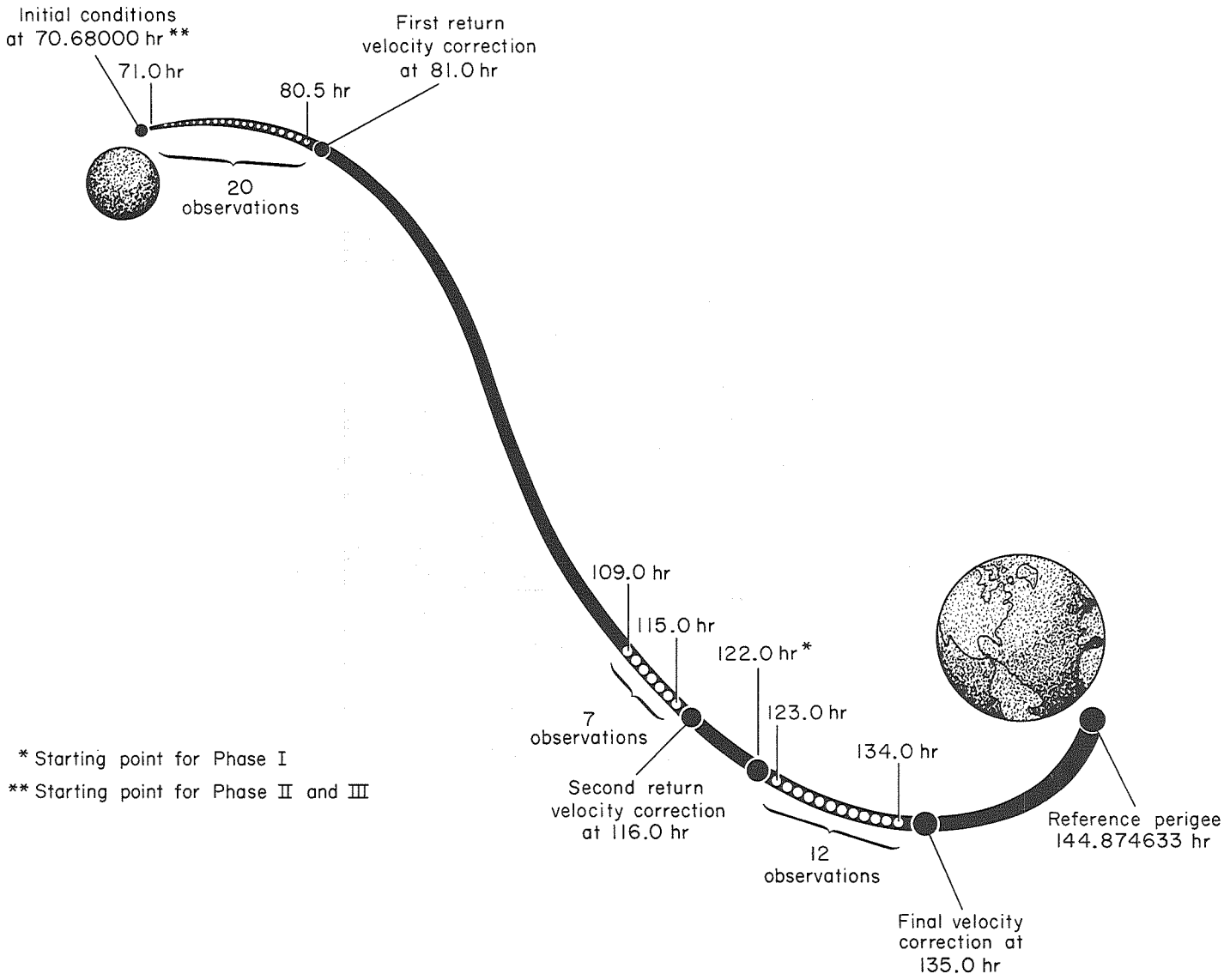

Figure 13.- Midcourse simulation return trajectory.

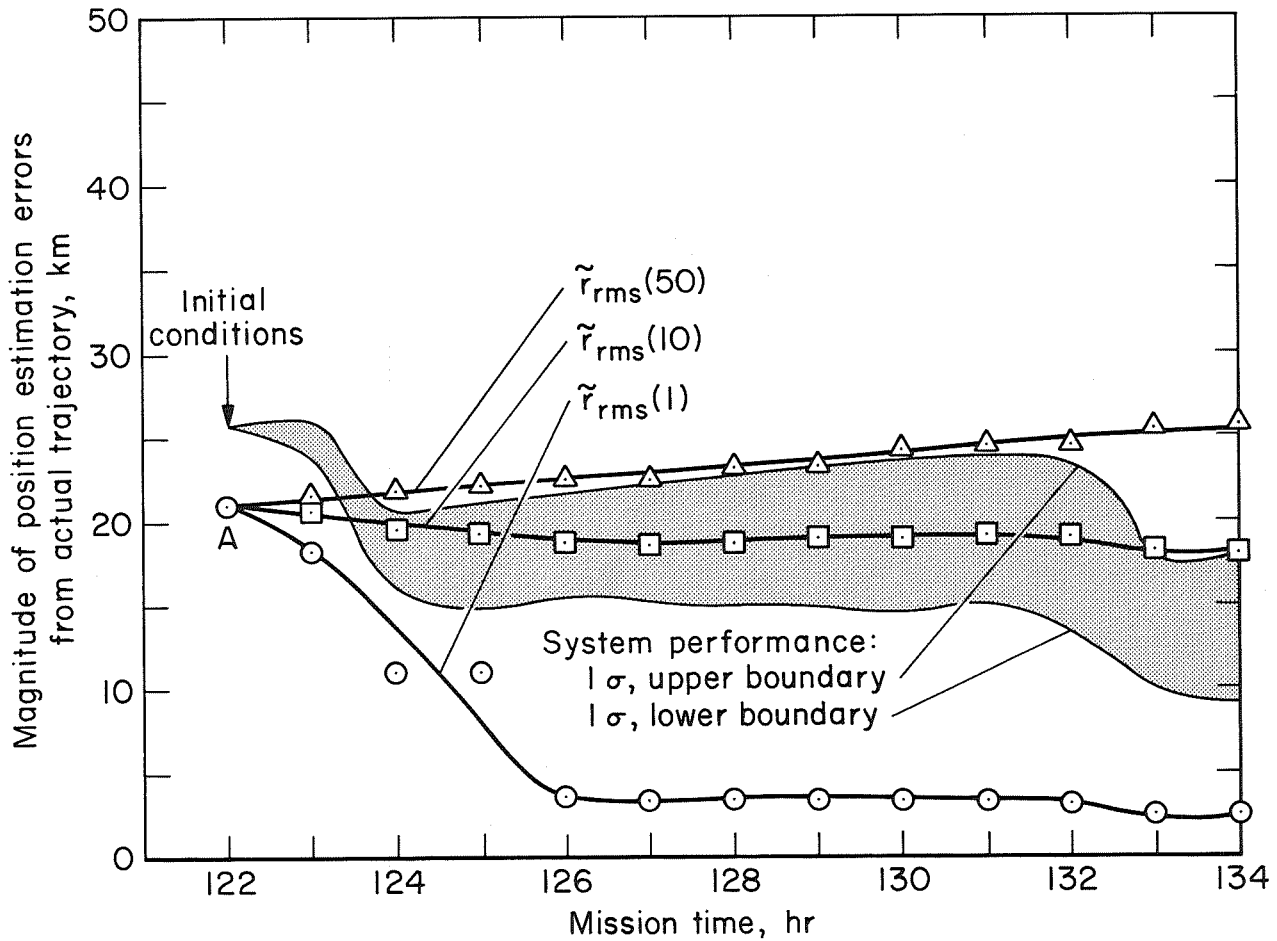

Figure 14.- Trajectory estimation errors, Phase I.

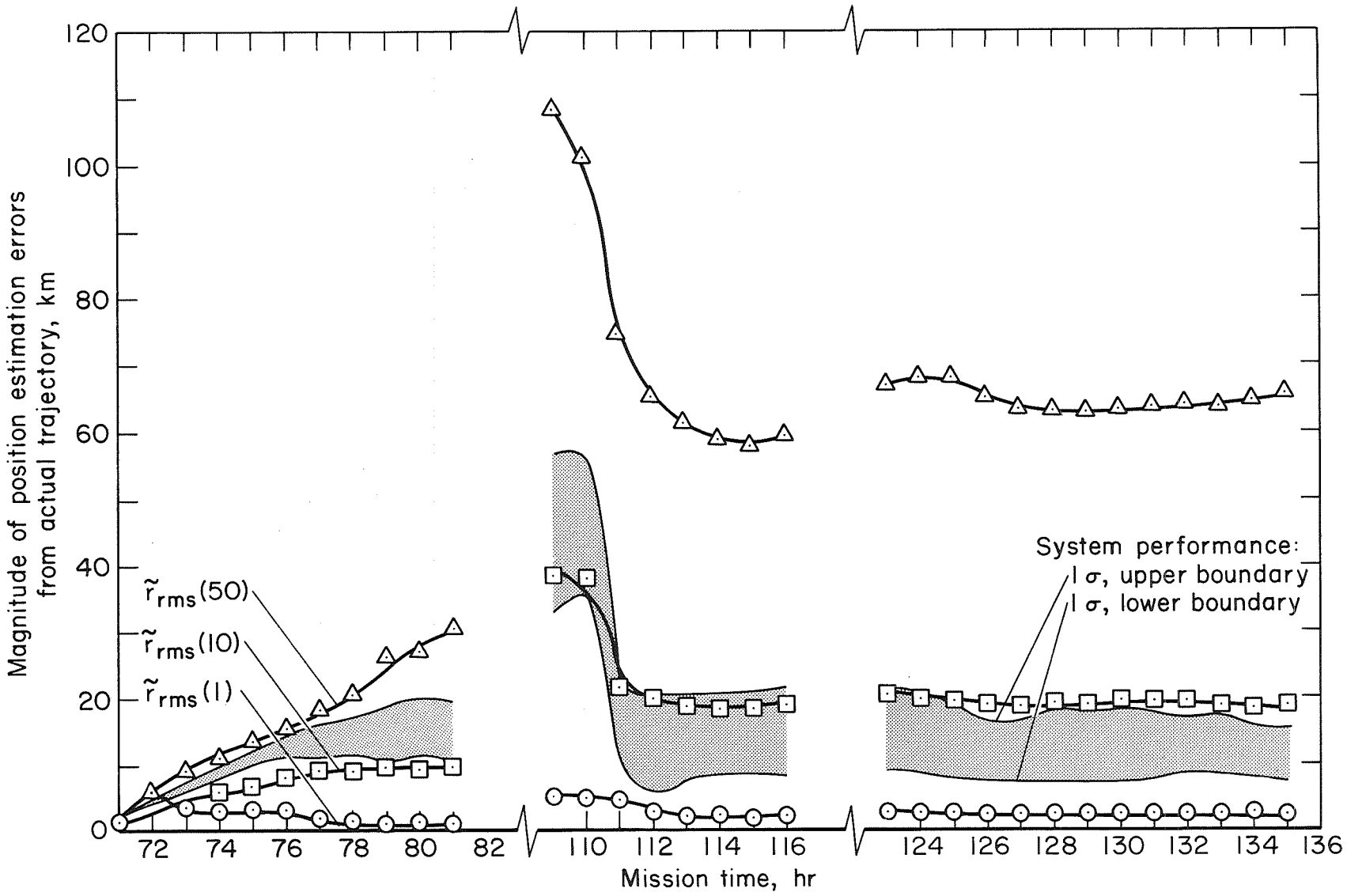

Figure 15.- Trajectory estimation errors, Phase II.

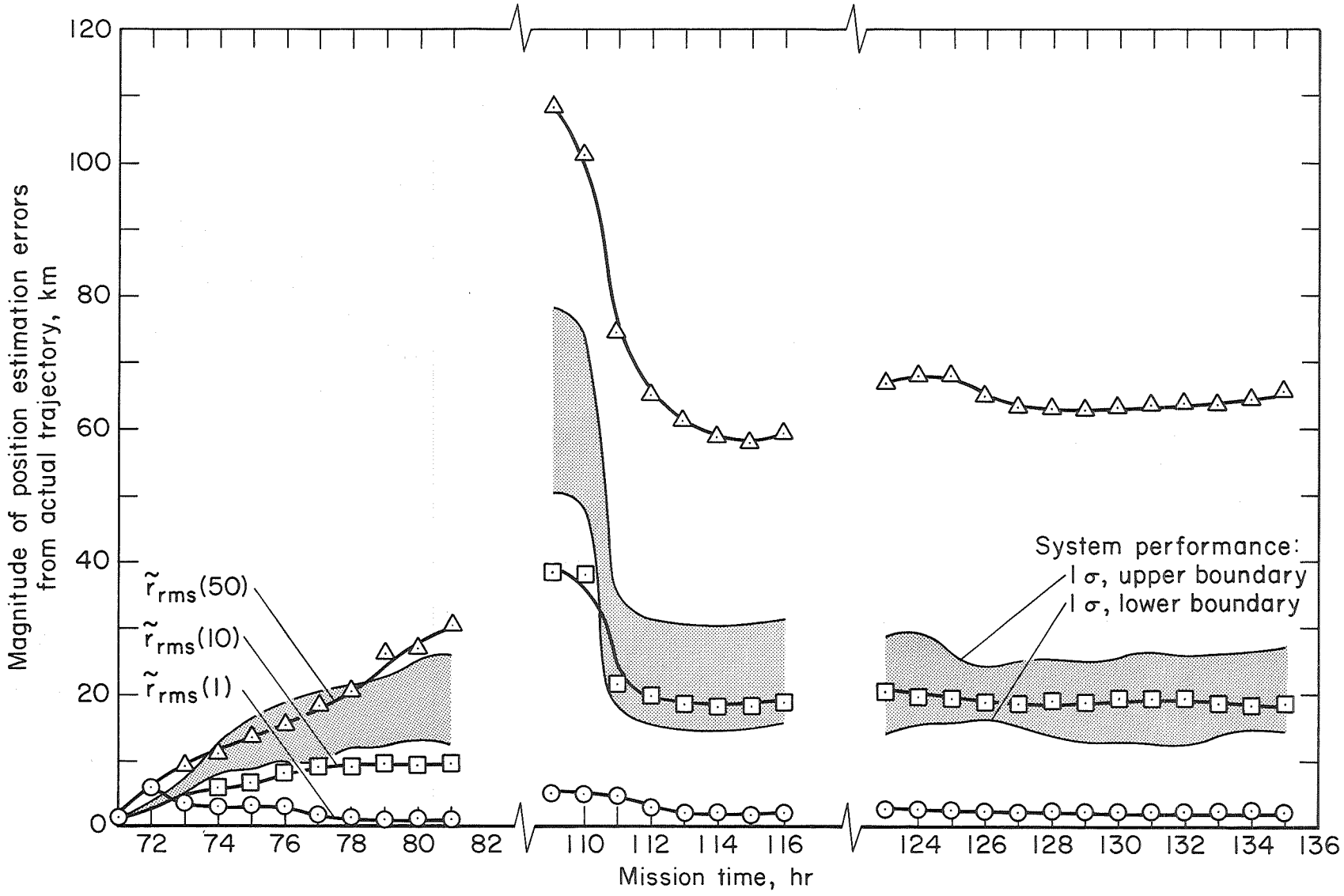

Figure 16.- Position estimation errors, Phase III.

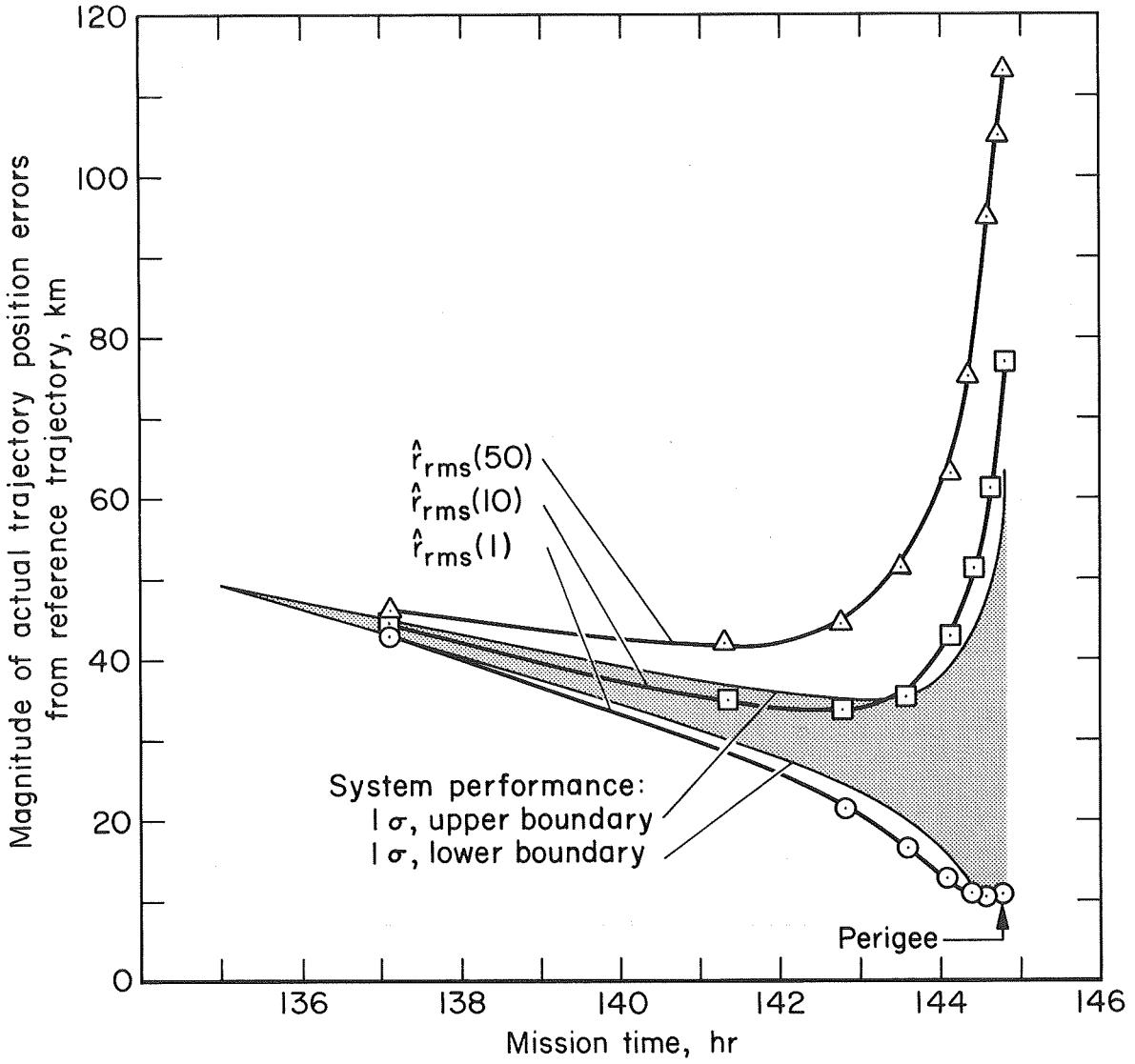

Figure 17.- Actual trajectory position errors, Phase I.

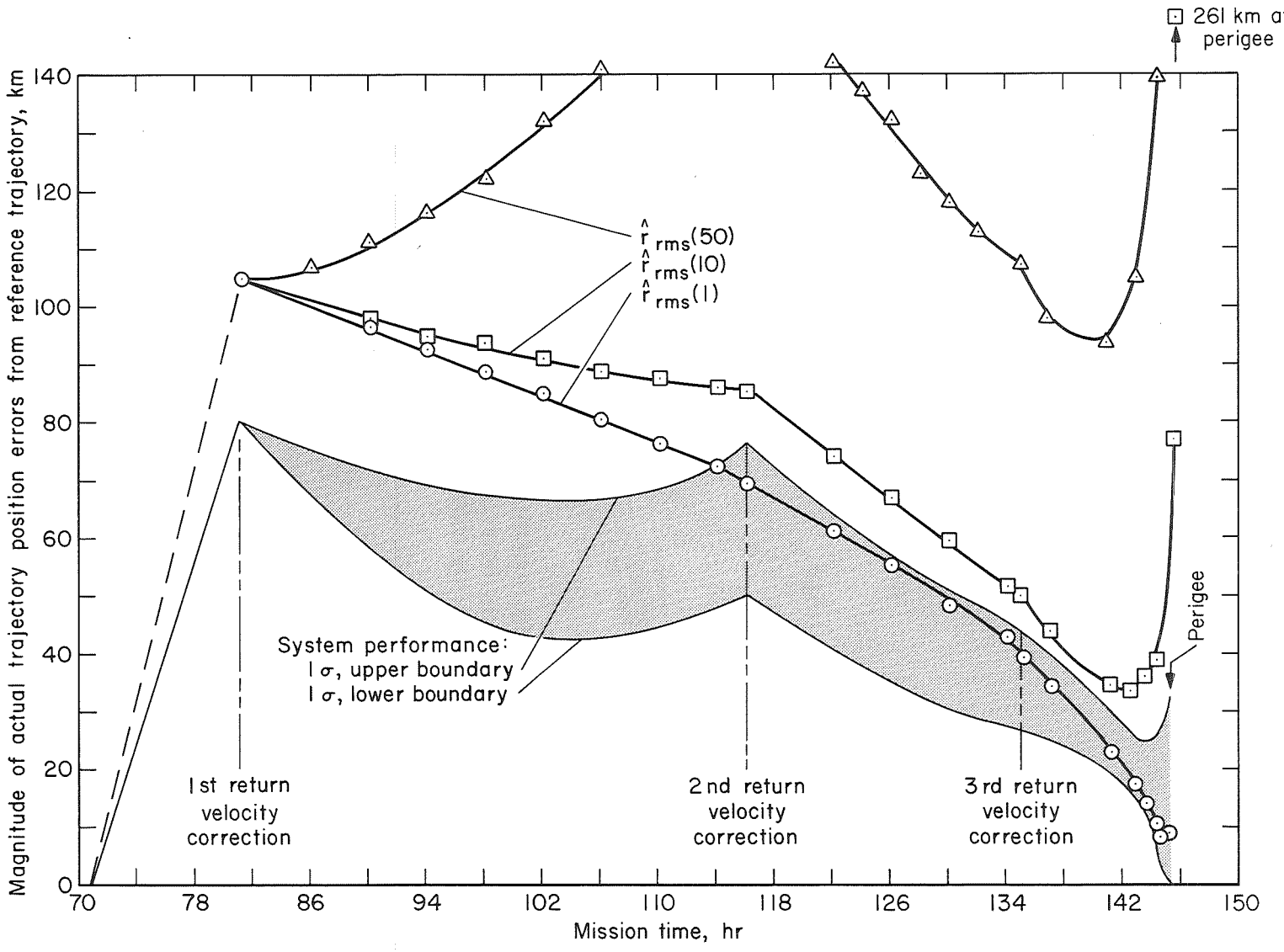

Figure 18.- Actual trajectory position errors, Phase II.

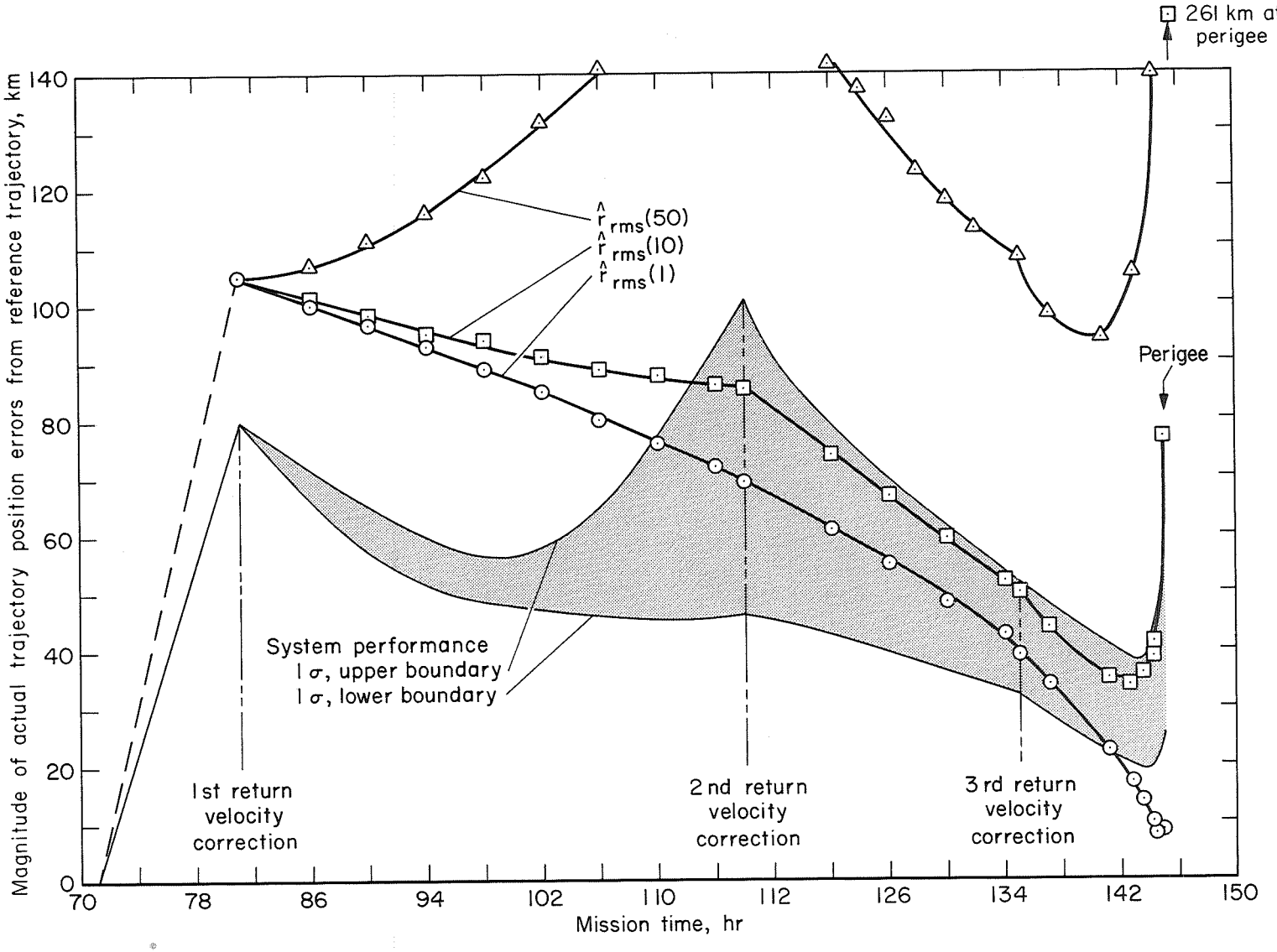

Figure 19.- Actual trajectory position errors, Phase III.

NATIONAL AERONAUTICS AND SPACE ADMINISTRATION
WASHINGTON, D. C. 20546
OFFICIAL BUSINESS

FIRST CLASS MAIL

POSTAGE AND FEES PAID
NATIONAL AERONAUTICS AN
SPACE ADMINISTRATION

POSTMASTER: If Undeliverable (Section 158 Postal Manual) Do Not Return

"The aeronautical and space activities of the United States shall be conducted so as to contribute . . . to the expansion of human knowledge of phenomena in the atmosphere and space. The Administration shall provide for the widest practicable and appropriate dissemination of information concerning its activities and the results thereof."

—NATIONAL AERONAUTICS AND SPACE ACT OF 1958

NASA SCIENTIFIC AND TECHNICAL PUBLICATIONS

TECHNICAL REPORTS: Scientific and technical information considered important, complete, and a lasting contribution to existing knowledge.

TECHNICAL NOTES: Information less broad in scope but nevertheless of importance as a contribution to existing knowledge.

TECHNICAL MEMORANDUMS: Information receiving limited distribution because of preliminary data, security classification, or other reasons.

CONTRACTOR REPORTS: Scientific and technical information generated under a NASA contract or grant and considered an important contribution to existing knowledge.

TECHNICAL TRANSLATIONS: Information published in a foreign language considered to merit NASA distribution in English.

SPECIAL PUBLICATIONS: Information derived from or of value to NASA activities. Publications include conference proceedings, monographs, data compilations, handbooks, sourcebooks, and special bibliographies.

TECHNOLOGY UTILIZATION PUBLICATIONS: Information on technology used by NASA that may be of particular interest in commercial and other non-aerospace applications. Publications include Tech Briefs, Technology Utilization Reports and Notes, and Technology Surveys.

Details on the availability of these publications may be obtained from:

SCIENTIFIC AND TECHNICAL INFORMATION DIVISION
NATIONAL AERONAUTICS AND SPACE ADMINISTRATION
Washington, D.C. 20546